

# Universal interface fluctuations in absorbing-state phase transitions

Yohsuke T. Fukai,<sup>1,2,3,\*</sup> Keiichi Tamai,<sup>3,4,5</sup> and Tetsuya Hiraiwa<sup>3,6,7,8,9</sup>

<sup>1</sup>*Nonequilibrium Physics of Living Matter Laboratory, RIKEN Pioneering Research Institute,  
2-2-3 Minatojima-minamimachi, Chuo-ku, Kobe, Hyogo 650-0047, Japan*

<sup>2</sup>*Nonequilibrium Physics of Living Matter Riken Hakubi Research Team,  
RIKEN Center for Biosystems Dynamics Research,  
2-2-3 Minatojima-minamimachi, Chuo-ku, Kobe, Hyogo 650-0047, Japan*

<sup>3</sup>*Department of Physics, The University of Tokyo,  
7-3-1 Hongo, Bunkyo-ku, Tokyo 113-0033, Japan*

<sup>4</sup>*Institute for Physics of Intelligence, The University of Tokyo,  
7-3-1 Hongo, Bunkyo-ku, Tokyo 113-0033, Japan*

<sup>5</sup>*The Institute for Solid State Physics, The University of Tokyo,  
5-1-5 Kashiwanoha, Kashiwa, Chiba 277-8581, Japan*

<sup>6</sup>*Institute of Physics, Academia Sinica, No. 128,  
Section 2, Academia Road, Taipei 11529, Taiwan*

<sup>7</sup>*Physics Division, National Center for Theoretical Sciences, Taipei 106319, Taiwan*

<sup>8</sup>*Mechanobiology Institute, National University of Singapore,  
5A Engineering Drive 1, Singapore 117411, Singapore*

<sup>9</sup>*Universal Biology Institute, The University of Tokyo,  
7-3-1 Hongo, Bunkyo-ku, Tokyo 113-0033, Japan*

(Dated: May 20, 2026)

Despite similarities between models exhibiting absorbing phase transitions (APTs) and those showing Kardar-Parisi-Zhang (KPZ) growth, the relationship between these universal fluctuations has remained elusive. We numerically study (1+1)-dimensional interfaces of (2+1)-dimensional models showing APTs of directed percolation (DP) and compact directed percolation (CDP) classes with an active boundary, finding a universal crossover from short-time APT-governed fluctuations to long-time KPZ fluctuations. Upon rescaling time and length by the APT correlation time and length, the cumulants of the interface height distributions collapse onto a single scaling function. The fluctuation properties of the discrete Domany-Kinzel model and the continuum stochastic Fisher-Kolmogorov-Petrovsky-Piskunov (sFKPP) equation coincide, indicating that the KPZ growth parameters are determined solely by fundamental properties of the APT. For the CDP sFKPP equation, a dimensionless parameter tunes both the critical interface distribution and the KPZ parameters, with the interface properties of the biased voter model recovered in a limiting case. These results uncover a universal crossover in which KPZ fluctuations emerge from APT fluctuations at long times, linking paradigmatic universality classes of nonequilibrium scale-invariant phenomena.

*Introduction.* Emergent scale invariance often leads to universal large-scale properties of fluctuations in nonequilibrium systems. Absorbing phase transitions (APTs) and interface growth are representative examples of such universality [1–6], and appear in various phenomena ranging from intermittent turbulence [7–9] to population dynamics [10–13], which can be described by local growth and competition. APTs, nonequilibrium phase transitions into absorbing states from which no transition to another state is possible [1–3], are examples where *bulk* scale invariance at the transition point leads to universal scaling laws for fluctuations. Here, the order parameter  $\rho(\mathbf{x}, t)$  evolves in  $d$ -dimensional space  $\mathbf{x} \in \mathbb{R}^d$ , and the system including the time axis is referred to as  $(d+1)$ -dimensional. The directed percolation (DP) class and the compact directed percolation (CDP) class are known as prototypical classes for cases with a single absorbing state and two symmetric absorbing states, respectively [1, 2]. On the other hand, when active clusters propagate and form fluctuating  $[(d-1)+1]$ -dimensional *interfaces* [4, 14], whose height  $h(\mathbf{x}, t)$ , i.e., the coarse-

grained position of such an interface at a dimensionally reduced spatial coordinate  $\mathbf{x} \in \mathbb{R}^{d-1}$ , often exhibits scale-invariant universal fluctuations which fall in a universality class. The Kardar-Parisi-Zhang (KPZ) universality class [3–6, 15] describes cases without special symmetries and conservation laws, and is found to be relevant in various systems [3]. Although each class is by now extensively studied, whether and how the two universalities are related has remained largely unaddressed.

A useful starting point is that several models are known to host both universal fluctuations in different parameter regimes. One of the earliest observations dates back at least to 1972, when Williams and Bjerknæs numerically studied [12] a version of the biased voter model, a model known to show the CDP-class transition, and discussed its connection to the Eden model in the off-critical limit [11], which describes interface growth in the KPZ class. Similarly, the off-critical limit of the contact process [1, 2, 10], a model showing the transition of the DP class, is identical to the Eden model [16]. Another example is the stochastic Fisher-Kolmogorov-

Petrovsky-Piskunov (sFKPP) equation [17–22] [Eq. (1)], which shows the DP- and CDP-class APTs [2, 17]. Interface fluctuations of discrete and continuous models associated with the (2+1)-dimensional sFKPP equation have been studied, and it has been established [16, 22, 23] that when the parameter is far from the critical value, the propagating wave front shows the fluctuations of the (1 + 1)-dimensional KPZ universality class.

In each of these examples, the two universalities live in distinct parameter regimes of a single model: APT criticality at the transition point, and KPZ interface growth far from it. When the control parameter is close to the critical point, one may expect an interface growth process characterized by both APT and KPZ universality [16]. However, no clear connection has been established between the universal properties of APT bulk fluctuations and those of the KPZ interface, nor between their characteristic temporal and spatial scales.

In this Letter, by simulating discrete and continuum models showing the DP- and CDP-class transitions, we reveal that the universality of APTs imposes strong constraints on the interface fluctuations of the noisy traveling waves. By rescaling length and time by the characteristic length and time of APTs, we find a universal crossover from a regime characterized by the APT exponents to that associated with the KPZ scaling, interconnecting the universal fluctuations.

*Models.* To investigate model-independent properties of interface fluctuations associated with APTs, we studied discrete and continuum models showing the (2 + 1)-dimensional DP- and CDP-class transitions. As the discrete models, we employed the bond percolation [1, 2, 24] for the DP class and the biased voter model (also called the Williams-Bjerknes model [12]) for the CDP class, which can be defined as a special case of the Domany-Kinzel (DK) model [1, 2, 25] on the (2+1)-dimensional body-centered cubic (BCC) lattice [24] (Fig. S1 [26]). In the model, the sites  $\rho((i, j), t)$  on a square lattice  $i = 0, \dots, L_x - 1, j = 0, \dots, L_y - 1$  at the time  $t$  take either the active [ $\rho((i, j), t) = 1$ ] or inactive [ $\rho((i, j), t) = 0$ ] state. The transition probability is determined by the percolation probability  $p$  and the bias  $\epsilon$  in the bond percolation and the biased voter model, respectively, as described in the End Matter [26].

As the continuum models, we simulated the sFKPP equation for the (2+1)-dimensional DP and CDP classes,

$$\frac{\partial \rho(\mathbf{x}, t)}{\partial t} = D \Delta \rho + A \rho - B \rho^2 + \sigma \sqrt{f(\rho)} \eta(\mathbf{x}, t), \quad (1)$$

where  $B = 1$  ( $A = B = \epsilon$ ) and  $f(\rho) = \rho$  [ $f(\rho) = \rho(1 - \rho)$ ] for the DP (CDP, respectively) class. We used the algorithm in Ref. [27] which ensures the nonnegativity of the density field. In this study, we used the lattice size  $\Delta x = 3$  and timestep size  $\Delta t = 0.25$ , with the system size written as  $L_x \Delta x \times L_y \Delta x$  [26].

Each model undergoes an absorbing-state phase transition at a critical parameter value [ $p = p_c$  (bond percolation),  $A = A_c$  (DP Langevin), and  $\epsilon = 0$  (CDP models); see Table AII and the End Matter for details [26]]. For the bond percolation and DP Langevin equation, we defined the distance from the transition point as  $\epsilon := (p - p_c) / p_c$  and  $\epsilon := (A - A_c) / A_c$ , respectively. Through simulations from homogeneous initial conditions, we further estimated the APT correlation time  $\xi_{\parallel}(\epsilon) \sim |\epsilon|^{-\nu_{\parallel}}$  and correlation length  $\xi_{\perp}(\epsilon) \sim |\epsilon|^{-\nu_{\perp}}$ , which diverge as  $\epsilon \rightarrow 0$  (Table AI; See End Matter and Figs. S2-S9 for the detailed methods and Tables SVI and SVII for the estimated parameters [26]).

*Interface fluctuation with active boundary.* We simulated the models with active walls to study the interface fluctuation [Figs. 1(a) and S10(a) [26]]. Specifically, the sites at the wall ( $y = 0$ ) were always set to active ( $\rho(\mathbf{x}, t) = \rho_b > 0$  for the Langevin equations, where  $\rho_b$  is a constant), and all other sites were initially set to inactive, after which the active region invaded [Figs. 1 and S10 [26]]. We defined the interface as the distance between the wall and the furthest active site (a lattice site with  $\rho(\mathbf{x}, t) > \rho_{th}$  for the Langevin equations [18, 19]) [Figs. 1(a,b) and S10(a,b) [26]].

The spanwise-averaged density showed a crossover from the critical-regime profile to that of a traveling wave around  $t \sim \xi_{\parallel}(\epsilon)$  [Figs. 1(c) and S10(c) [26]], confirming that  $\xi_{\parallel}(\epsilon)$  is also the characteristic timescale for the interface dynamics; the interface morphology and height distribution function likewise qualitatively changed around  $\xi_{\parallel}(\epsilon)$  [Figs. 1(b,d) and S10(b,d) [26]].

To quantify this crossover, we calculated the cumulants  $\langle h(x, t)^k \rangle_c$  ( $k = 1, 2, 3, 4$ ) for the discrete models and found consistent behavior across  $\epsilon$  values (Fig. S11 [26]). Interfaces at criticality ( $\epsilon = 0$ ) exhibited power-law growth with the APT dynamic exponent  $\langle h^k \rangle_c \sim t^{k/z^{(C)DP}}$ , while for large  $\epsilon$  a temporal region emerged in which the KPZ-class exponents were observed;  $\langle h^k \rangle_c \sim t$  ( $k = 1$ ) and  $\langle h^k \rangle_c \sim t^{k\beta^{KPZ}}$  ( $k > 1$ ), where  $\beta^{KPZ} = 1/3$  is the growth exponent for the KPZ class (Table AI [26]). This KPZ regime appeared at progressively earlier times as  $\epsilon$  increased. These observations motivate rescaling the height, time, and spatial coordinate by the characteristic length and temporal scales of the APT,  $\xi_{\perp}(\epsilon)$ ,  $\xi_{\parallel}(\epsilon)$ , and  $\xi_{\perp}(\epsilon)$ , respectively.

*Universal crossover from APT to KPZ-class fluctuation.* We rescaled the height, time, and spatial coordinate as

$$h_{\xi}(x_{\xi}, t_{\xi}) := h(x, t) / \xi_{\perp}(\epsilon), \quad t_{\xi} := t / \xi_{\parallel}(\epsilon), \quad x_{\xi} := x / \xi_{\perp}(\epsilon), \quad (2)$$

and found that the cumulants collapse onto unique scaling functions bridging the APT and KPZ regimes (Fig. 2). These functions show the asymptotic APT scaling laws in the region  $t_{\xi} \ll 1$  (the short-time regime) and

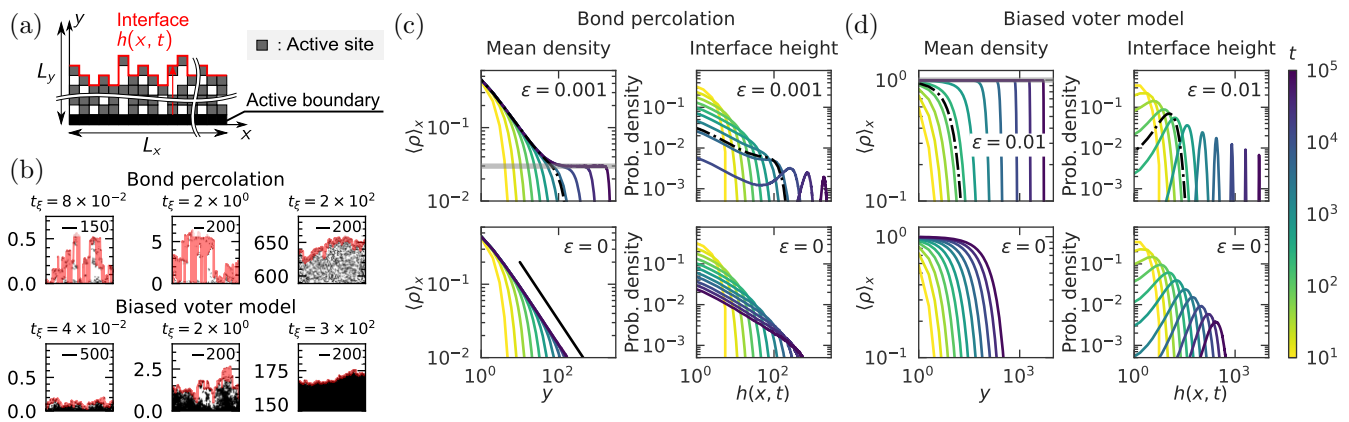


FIG. 1: Schematic and qualitative illustration of the interface growth process in the discrete models. (a) An illustration of the height definition for the discrete models with the active boundary. (b) Example snapshots of the active sites (black field) and the interface (red line) for the bond percolation (upper) and biased voter model (lower), respectively. The axis label and the scale bar indicate the length rescaled by the correlation length  $\xi_{\perp}(\epsilon)$  and the actual length, respectively. The rescaled time  $t_{\xi} = t/\xi_{\parallel}(\epsilon)$  is denoted in each plot. The values of  $\epsilon$  are  $1 \times 10^{-5}$ ,  $1 \times 10^{-4}$  and  $5 \times 10^{-3}$  for the bond percolation and  $1 \times 10^{-6}$ ,  $5 \times 10^{-5}$  and  $5 \times 10^{-3}$  for the biased voter model, respectively. (c,d) The spanwise-averaged density  $\langle \rho(\mathbf{x}, t) \rangle_x$  (left) and height probability distribution (right) for the bond percolation (c) and biased voter model (d), respectively. The top and bottom plots are the off-critical and critical cases, respectively. The dash-dot lines are the data at  $t \approx \xi_{\parallel}(\epsilon)$ . The gray lines in the off-critical mean-density plots indicate  $\rho_{\infty}(\epsilon)$  (bond percolation) and 1 (biased voter model). The black line in the left bottom plot of (c) indicates the power law  $\langle \rho(\mathbf{x}, t) \rangle_x \propto y^{-\beta^{\text{DP}}/\nu_{\perp}}$ .

the KPZ scaling laws in  $t_{\xi} \gg 1$  (the long-time regime), suggesting

$$\langle h_{\xi}(x_{\xi}, t_{\xi})^k \rangle_c \simeq g_k(t_{\xi}), \quad g_k(t_{\xi}) \sim \begin{cases} t_{\xi}^{k/z^{(\text{C})\text{DP}}} & (t_{\xi} \ll 1) \\ t_{\xi} & (t_{\xi} \gg 1, k = 1) \\ t_{\xi}^{k\beta^{\text{KPZ}}} & (t_{\xi} \gg 1, k > 1). \end{cases} \quad (3)$$

Interfaces at criticality ( $\epsilon = 0$ ) exhibited the same scaling laws as those observed in the short-time limit (Fig. S11 [26]).

The skewness  $\text{Sk}[h_{\xi}] := \langle h_{\xi}^3 \rangle_c / \langle h_{\xi}^2 \rangle_c^{3/2}$  and the kurtosis  $\text{Ku}[h_{\xi}] := \langle h_{\xi}^4 \rangle_c / \langle h_{\xi}^2 \rangle_c^2$  exhibited plateaus in both the short- and long-time limits (Fig. 2), indicating the existence of asymptotic height distributions in each regime. In the short-time regime, the plateau values agreed with those obtained at criticality ( $\epsilon = 0$ ), where both quantities remained constant over a long timescale (Fig. S12 [26]), suggesting that the height distribution converges to a well-defined critical distribution. In the long-time regime, both values converged to those of the Gaussian orthogonal ensemble Tracy–Widom (GOE–TW) distribution, the exact solution for the KPZ class with a flat initial condition. This convergence further confirmed the emergence of the KPZ-class fluctuation.

*Universality of height fluctuation.* Comparison between the discrete models and the Langevin equations revealed the universality of the height fluctuation across models. At criticality ( $\epsilon = 0$ ), the height distributions of

the Langevin equations, rescaled by the dynamic correlation length, asymptotically converged to those of the critical bond percolation, irrespective of the threshold  $\rho_{th}$ ; the cutoffs at  $y > 0$  observed with smaller  $\rho_{th}$  or larger  $\rho_b$  values decreased as time increased [Figs. 3 (left) and S13 [26]], suggesting the existence of a universal asymptotic height distribution for models in the DP class. Similarly, for the CDP Langevin equation, the moderate effect of  $\rho_{th}$  disappeared in the long-time limit [Figs. 3 (right) and S14 [26]]. At  $D/\sigma^2 \ll 1$ , the distribution function overlapped with that for the biased voter model, confirming the universality of the critical height distribution (Figs. A1 and S15 [26]). Interestingly, at larger  $D/\sigma^2$ , the asymptotic height distribution retained almost the same shape but was shifted (Figs. A1, S14 and S15 [26]), suggesting that the dimensionless parameter  $D/\sigma^2$ , which is marginal at  $d = 2$  under rescaling of space and time, has a fundamental effect on the critical height distribution even after rescaling by the diverging CDP correlation length.

This universality extended to the off-critical regime. For  $\epsilon > 0$ , the cumulants of the Langevin equations collapsed onto the same scaling functions as those of the discrete models under conditions where the critical height distributions matched (Figs. 2 and S16 [26]). For the CDP Langevin equations, the cumulant scaling functions depended slightly on  $D/\sigma^2$ , further supporting the role of  $D/\sigma^2$  as a fundamental parameter governing the large-scale behavior (Fig. S17 [26]).

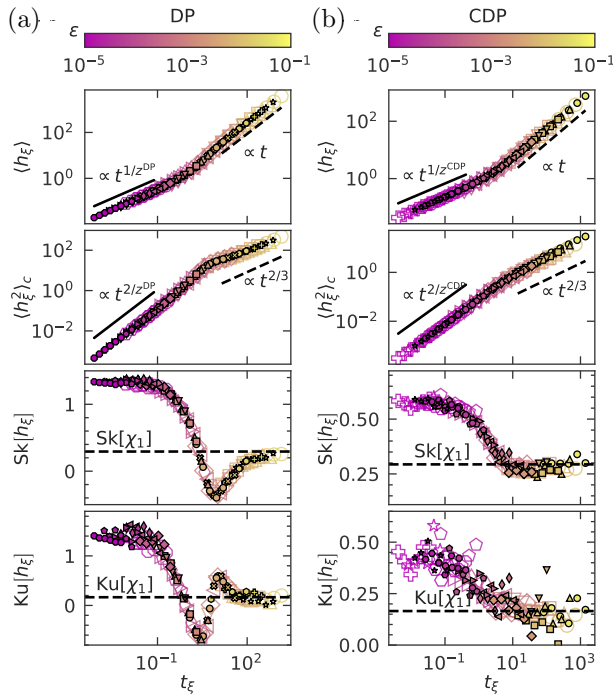


FIG. 2: Cumulants and cumulant ratios of the height distribution function for the (a) DP- and (b) CDP-class models. The plots show the mean, variance, skewness, and kurtosis for the rescaled height  $\langle h_\xi \rangle$ ,  $\langle h_\xi^2 \rangle_c$ ,  $Sk[h_\xi]$  and  $Ku[h_\xi]$  for the off-critical cases. The larger unfilled and smaller filled symbols are for the discrete models and the Langevin equations [ $D = 1$ ,  $\sigma = 1$ ,  $\rho_b = 0.1$ , and  $\rho_{th} = 0.1$  (DP) and  $D = 0.1$ ,  $\sigma = 1$ ,  $\rho_b = 1$ , and  $\rho_{th} = 0$  (CDP)], respectively. The solid and dashed lines in the upper two plots are guides for the eye for the APT and KPZ exponents (see the main text), respectively. The dashed lines in the lower two plots show the theoretical values for the GOE-TW distribution,  $\chi_1$ .

*KPZ growth with universal parameters.* In the KPZ regime, the asymptotic height is described by

$$h_\xi(x_\xi, t_\xi) \simeq v_\infty t_\xi + (\Gamma t_\xi)^{\beta_{\text{KPZ}}} \chi(X) \quad (t_\xi \rightarrow \infty), \quad (4)$$

with  $X := x_\xi / \xi^{\text{KPZ}}(t_\xi)$  and  $\xi^{\text{KPZ}}(t_\xi) := \frac{2}{A} (\Gamma t_\xi)^{1/z^{\text{KPZ}}}$ , where  $z^{\text{KPZ}} = 3/2$  is the dynamical exponent for the KPZ class (Table AI [26]),  $\chi(X)$  is the universal stochastic variable, and  $v_\infty$ ,  $\Gamma$ , and  $A$  are system-dependent parameters [6, 28, 29]. These parameters can be estimated from the height cumulants following standard methods [6, 30, 31] (See the End Matter [26]).

Owing to the universality of the height fluctuation scaled by the APT correlation time and length, we expect these parameter values to be universal, in the sense that they only depend on the fundamental properties of the APT irrespective of the system details. We found that the estimated parameters for the bond percolation

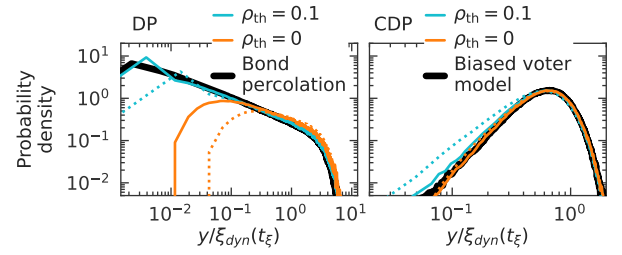


FIG. 3: The critical height distribution for the (left) DP-class and (right) CDP-class models. Data for the discrete models (black solid lines) and the Langevin equations [ $\rho_b = 0.1$  for the left and  $\rho_b = 1$  for the right] are shown. The dashed and solid curves show the data at  $t = 1 \times 10^4$  and  $t = 1 \times 10^5$ , respectively.

and DP Langevin equation indeed agree within the uncertainties, supporting the idea of KPZ growth with universal parameters (Fig. S18 and Tables AIII and SVIII [26]). For the CDP models, in accordance with the observation that the critical height distribution depends on the dimensionless parameter  $D/\sigma^2$ , the KPZ parameters were also dependent on  $D/\sigma^2$  for the Langevin equation and agreed with those for the biased voter model with small  $D/\sigma^2$ , suggesting its universality (Fig. S18 and Table SVIII [26]). In the original scale of  $h(x, t)$ , the parameters, denoted by  $v'_\infty$ ,  $\Gamma'$ , and  $A'$ , follow

$$v'_\infty = v_\infty \frac{\xi_{\parallel}(\epsilon)}{\xi_{\perp}(\epsilon)}, \quad \Gamma' = \Gamma \frac{\xi_{\perp}(\epsilon)^3}{\xi_{\parallel}(\epsilon)}, \quad A' = A \xi_{\perp}(\epsilon), \quad (5)$$

which leads to the power laws for the KPZ parameters  $v'_\infty \sim \epsilon^{\nu_{\perp} - \nu_{\parallel}}$ ,  $\Gamma' \sim \epsilon^{\nu_{\parallel} - 3\nu_{\perp}}$ , and  $A' \sim \epsilon^{-\nu_{\perp}}$ .

When rescaled by the dynamical correlation length  $\xi_{\text{dyn}}(t)$  in the short-time regime and by the KPZ parameters as  $\frac{h_\xi(x_\xi, t_\xi) - v_\infty t_\xi}{(\Gamma t_\xi)^{1/3}}$  in the long-time regime [Eq. (4)], the height distributions collapsed onto unique curves in both limits (Figs. S19 and S20 [26]). In the short-time regime, the height histograms converged to that of the critical interfaces ( $\epsilon = 0$ ). In the long-time regime, the height distribution agreed with the exact solution for the KPZ class with the flat initial condition, the GOE-TW distribution. We also found consistent behavior for the height spatial covariance  $C_{s,int}(l, t_\xi) := \text{Cov}[h_\xi(x_\xi + l, t_\xi), h_\xi(x_\xi, t_\xi)]$  (End Matter; Figs. S21 and S22 [26]).

*Discussion and conclusion.* We investigated the fluctuations of interfaces defined by the farthest active sites from the active boundary in the models exhibiting APTs of the DP and CDP classes. By rescaling the spatial and temporal scales by the APT correlation length and time, respectively, we found a universal crossover from height fluctuations characterized by the APT dynamical correlation length and the statistical properties of the critical interfaces to those of the KPZ class. The scaling function was found to be robust, with its long-time limit

independent of the model details and of the threshold  $\rho_{th}$  used to define the interface in the Langevin cases. The result suggests that one can predict the statistical properties of the interfaces solely from the bulk correlation length and time, and conversely that properties of the critical fluctuation in the bulk can be inferred from the evolution of the interface fluctuation. Interestingly, for the CDP Langevin equation, the dimensionless parameter  $D/\sigma^2$  tuned both the critical fluctuation properties and the KPZ-interface parameters. The results showed agreement with the biased voter model in the limit  $D/\sigma^2 \rightarrow 0$ .

Our results show that the KPZ fluctuation emerges from APT fluctuations in the long-time limit. It would be interesting to explore whether this crossover scenario of “nested” universal fluctuations can be generalized to other classes of APTs [1, 2]. Furthermore, understanding the circumstances that determine the interface fluctuation would be important, given that the interface fluctuations associated with the Ginzburg-Landau equation have been reported to exhibit Edwards-Wilkinson-class fluctuations [32]. The effect of noise in the sFKPP equation has been extensively studied [22], and a unified understanding bridging our results with those obtained in its strong-noise limit [33] would be another interesting direction. Another open question is whether the critical APT-associated interface fluctuation shows geometry dependence analogous to that of the KPZ class [5, 6, 28, 34].

Experimental realizations in phenomena associated with APTs [3, 9, 35] or in neighbor interactions analogous to the voter model [36] would also be valuable to pursue. Notably, the DP-class APT and the KPZ-class interface growth have both been experimentally observed in similar setups of liquid crystal electroconvection [3, 29, 35], making this system a promising candidate to probe the crossover predicted here. The KPZ growth with universal parameters is expected at temporal and spatial scales  $t$  and  $l$  satisfying  $t_{\text{micro}} \ll \xi_{\parallel}(\epsilon) \ll t$  and  $l_{\text{micro}} \ll \xi_{\perp}(\epsilon) \ll l$ , where  $t_{\text{micro}}$  and  $l_{\text{micro}}$  denote the microscopic time and length scales of the dynamics. This regime is accessible, for example, in the DSM1–DSM2 transition of electroconvecting liquid crystals [35], for which the APT correlation time and length,  $\xi_{\parallel}(\epsilon) \approx 5$  s and  $\xi_{\perp}(\epsilon) \approx 100 \mu\text{m}$  at  $\epsilon = 10^{-2}$ , lie below the typical experimental observation windows [37].

We thank Hiroki Yamaguchi for the preliminary simulations and discussions on the exact expressions in the CDP cases. We acknowledge valuable discussion with Kazumasa A. Takeuchi, Kyogo Kawaguchi, Kyosuke Adachi, Rory Cerbus, Takeyuki Miyawaki and Somayeh Zeraati. We are grateful to Michael Prähofer and Herbert Spohn for the theoretical curves of the GOE Tracy–Widom distribution, which are made available online [38], and to Folkmar Bornemann for the curves of the  $\text{Airy}_1$  covariance, evaluated by his algorithm in [39]. This work is supported in part by KAKENHI from Japan Society

for the Promotion of Science (Grant Nos. JP17J05559, JP22K14016, 19H05795, and 25H01360) and JST ACT-X grant number JPMJAX24LF (to Y.T.F.) and the Seed fund of Mechanobiology Institute (to T.H.). We thank the Supercomputer Center of the Institute for Solid State Physics (the University of Tokyo), the Meiji Institute for Advanced Study of Mathematical Sciences (Meiji University) and the Center for Computational Sciences (University of Tsukuba) for computational resources.

## END MATTER

TABLE AI: Values of universal exponents [1, 2]. For the DP class, we used the values estimated in Ref. [24].

Name	$\beta^{\text{DP}}$	$\nu_{\parallel}^{\text{DP}}$	$\nu_{\perp}^{\text{DP}}$	$\beta^{\text{CDP}}$	$\beta'^{\text{CDP}}$	$\nu_{\parallel}^{\text{CDP}}$	$\nu_{\perp}^{\text{CDP}}$
Value	0.580(4)	1.287(2)	0.729(1)	0	1	1	1/2

TABLE AII: Values of the critical parameters for the DP models. For the bond percolation, we used the values estimated in [24].

Model	Bond percolation	DP Langevin
Name	$p_c$	$A_c$
Value	0.28733837(2)	0.181358(4)

TABLE AIII: Estimated parameters of the KPZ class in the long-time regime (excerpt). For the Langevin equations, the data for  $D = 1, \sigma = 1, \rho_b = 0.1$  (DP) and  $D = 0.1, \sigma = 1, \rho_b = 1$  (CDP) are shown, respectively. The ‘‘Value’’ column indicates the value estimated with the values of the APT nonuniversal parameters shown in Table SVI and SVII, and the ‘‘Max’’ and ‘‘Min’’ columns indicate the maximum and minimum values obtained by varying the APT nonuniversal parameters within the uncertainties, respectively. In the ‘‘Value’’ column, the statistical uncertainties are shown in parentheses. The full table is shown in Table SVIII [26]. The values are also shown in Fig. S18 [26] as a plot.

model	$v_{\infty}$			$\Gamma$		
	Value	Max	Min	Value	Max	Min
Bond percolation	2.756(3)	2.894	2.627	14.2(1)	16.8	12.1
DP Langevin	2.84(1)	3.00	2.70	15.1(5)	18.5	12.5
Biased voter	0.539(3)	0.557	0.523	0.132(3)	0.150	0.120
CDP Langevin	0.535(1)	0.561	0.510	0.146(3)	0.179	0.125

### Transition probability for discrete models

In the discrete models,  $\rho((i, j), t + 1)$  becomes active with the probability  $p_k$ , where  $k$  is the number of connected active sites at the previous step [40] (Fig. S1 [26]). For the bond percolation model, we set  $p_k = 1 - (1 - p)^k$  where  $p$  is the probability with which the active states propagate [2, 24]. For the biased voter model, we employed a parallel-update version in which the two halves of the sites are alternately updated in a checkerboard

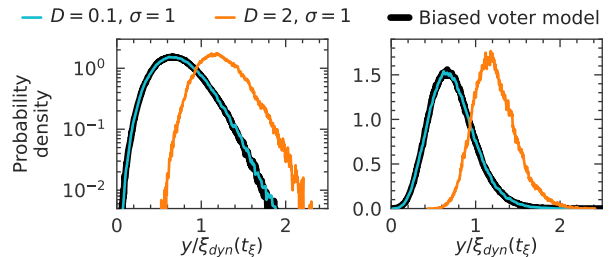


FIG. A1: The critical height distribution for the CDP-class models with different  $D/\sigma^2$  values. Full data are shown in Fig. S15.

pattern [26]. The site state changes to that of a randomly chosen nearest-neighbor site selected with biased probabilities  $(1 + \frac{\epsilon}{2})$  (active site) and  $(1 - \frac{\epsilon}{2})$  (inactive site), which leads to  $p_k = \frac{(2+\epsilon)k}{8+2\epsilon(k-2)}$  [26].

### Nonuniversal parameter estimation

#### Simulation with homogeneous initial condition

We estimated the model-dependent nonuniversal parameters for APTs by performing simulations with homogeneous initial conditions. The initial conditions were set as (a1) the all-active initial condition for the bond percolation, (a2) the random initial condition for the biased voter model where each site is independently set to active or inactive with probability 1/2, and (b)  $\rho(\mathbf{x}, t) = \rho_{\text{init}} = 10$ (DP), 0.5(CDP) for the Langevin equation. The estimated parameters are summarized in Table SVI and SVII.

### Critical parameters of DP models

The bond percolation model showed the transition at the critical value of  $p$  estimated in Ref. [24] [Table AII, Fig. S2 (a,b) [26]]. For the DP Langevin equation, we estimated the critical value by finding a value of  $A$  with which the mean order parameter  $\langle \rho(\mathbf{x}, t) \rangle$  decays algebraically as  $\sim t^{-\beta^{\text{DP}}/\nu_{\parallel}^{\text{DP}}}$  in a simulation with a homogeneous initial condition [26], where  $\beta^{\text{DP}}$  and  $\nu_{\parallel}^{\text{DP}}$  are universal exponents for the DP class [Table AI, Table AII; Fig. S2 (c-e) [26]].

### Characteristic timescales

For the DP models, we estimated the correlation time  $\xi_{\parallel}(\epsilon)$  by fitting the decay of the mean order parameter to  $\propto \exp[-t/\xi_{\parallel}(\epsilon)]$ , and then extracted  $t_0$  from the scaling form  $\xi_{\parallel}(\epsilon) := t_0 \epsilon^{-\nu_{\parallel}^{\text{DP}}}$ . The stationary density  $\rho_{\infty}(\epsilon)$  was

obtained from the long-time value of  $\langle \rho(\mathbf{x}, t) \rangle$  for  $\epsilon > 0$  [26]. Rescaling  $t$  and  $\rho(\mathbf{x}, t)$  by  $\xi_{\parallel}(\epsilon)$  and  $\rho_{\infty}(\epsilon)$ , respectively, produced a scaling collapse of  $\langle \rho(\mathbf{x}, t) \rangle$  (Fig. S3 [26]).

For the CDP models, we first fitted an exponential function  $C_{t0} \exp[-t/\xi_{\parallel}(\epsilon)]$  to the tail of the mean density  $1 - \langle \rho(\mathbf{x}, t) \rangle$  for  $\epsilon > 0$ , where  $C_{t0}$  is a constant that depends on the value of  $\epsilon$  and  $\xi_{\parallel}(\epsilon)$  is the correlation time. By plotting the values of  $\xi_{\parallel}(\epsilon)$  against  $\epsilon$ , we noticed a linear relationship between  $\xi_{\parallel}(\epsilon)\epsilon$  and  $\log \xi_{\parallel}(\epsilon)$ , in agreement with the theoretical expectation [41]. We then fitted a linear function to those values for the parameters shown in Fig. S4 to estimate the parameters  $C_1$  and  $C_2$  for the relationship  $\epsilon \xi_{\parallel}(\epsilon) = C_1 + C_2 \ln \xi_{\parallel}(\epsilon)$ , which are used to calculate the correlation time for general  $\epsilon$  as  $\xi_{\parallel}(\epsilon) = -\frac{C_2}{\epsilon} W_{-1} \left[ -\frac{\epsilon}{C_2} \exp\left(-\frac{C_1}{C_2}\right) \right]$ , where  $W_{-1}$  is the lower branch of the Lambert  $W$  function [26]. The estimated parameters are summarized in Table SVII and Fig. S5 [26]. Interestingly, we found that the value of  $C_2$  depends on the dimensionless parameter  $D/\sigma^2$  (Fig. S5 [26]). Rescaling the mean density by the estimated correlation time collapsed the data for different  $\epsilon$  values onto a single curve (Fig. S6 [26]).

### Characteristic length scales

We then estimated the correlation length  $\xi_{\perp}(\epsilon)$  as follows. For the DP models, we fitted an empirical function [2, 37]

$$\tilde{C}(\hat{l}) = C_{s0} \hat{l}^{-(\beta^{\text{DP}}/\nu_{\perp}^{\text{DP}})} e^{-\hat{l}}, \quad (\text{A1})$$

where  $\hat{l} := l/\xi_{\perp}(\epsilon)$  and  $\xi_{\perp}(\epsilon) := x_0 \epsilon^{-\nu_{\perp}^{\text{DP}}}$ , to the stationary rescaled spatial covariance  $C_s(l, t \gg \xi_{\parallel}(\epsilon))/\rho_{\infty}(\epsilon)^2$ , where  $C_s(l, t) := \text{Cov}[\rho(\mathbf{x} + l\mathbf{e}, t), \rho(\mathbf{x}, t)]$ ,  $\text{Cov}[A, B]$  is the covariance between  $A$  and  $B$ , and  $\mathbf{e}$  is a unit vector (Fig. S7 [26]).

For the CDP models, we defined the correlation length using the dynamic correlation length at criticality ( $\epsilon = 0$ ), because the stationary state is trivial unless  $\epsilon = 0$ . Specifically, we fitted the scaled exact solution [42, 43]

$$C_{\text{dyn}} [\ln(t/t_0)]^{-1} \text{Ei}_1 \left[ l^2 / \xi_{\text{dyn}}(t)^2 \right], \quad (\text{A2})$$

where  $\text{Ei}_1(x) := \int_0^{\infty} w^{-1} e^{-w} dw$ ,  $\xi_{\text{dyn}}(t) := (D't)^{1/z^{\text{CDP}}}$ , and  $z^{\text{CDP}} := \nu_{\parallel}^{\text{CDP}}/\nu_{\perp}^{\text{CDP}} = 2$  to the spatial covariance  $C_s(l, t)$  at criticality to find the dynamic correlation length  $\xi_{\text{dyn}}(t)$ , and then defined the correlation length by  $\xi_{\perp}(\epsilon) := \xi_{\text{dyn}}(\xi_{\parallel}(\epsilon))$  (Figs. S8 and S9 [26]). The  $C_s(l, t)$  rescaled by the scaling ansatz agreed with the exact function with the maximum deviation  $\approx 0.5$  (Fig. S8 [26]). We found that  $D'$  depends roughly linearly on  $D$  as  $D' \approx 7.7(1) \times D$  (Fig. S9 [26]).

### Parameter estimation for the KPZ interfaces in the long-time limit

We estimated the parameters for the KPZ interfaces following a standard method [6, 30, 31]. In short, we fitted a linear function to  $\left\langle \frac{\partial h_{\xi}}{\partial t_{\xi}} \right\rangle$  versus  $t_{\xi}^{-2/3}$  to estimate  $v_{\infty}$  from the intercept, and similarly fitted  $t_{\xi}^{-2/3} \langle h_{\xi}^2 \rangle_c$  versus  $t_{\xi}^{-2/3}$  to estimate  $\Gamma$  from the intercept, assuming that  $\chi$  in Eq. (4) follows the GOE-TW distribution. We then calculated  $A$  using  $\Gamma = \frac{A^2 v_{\infty}}{2}$  [6]. The estimated parameters are summarized in Fig. S18 and Table SVIII [26]. The data for  $t > 5 \times 10^3$  were used for the fitting, and the fitting was not attempted if there were fewer than 10 data points in the fitting range.

Specifically, for the  $v_{\infty}$  estimation, we approximated the derivative  $\left\langle \frac{\partial h_{\xi}}{\partial t_{\xi}} \right\rangle$  by the finite difference of the mean height  $\langle h_{\xi} \rangle$  at  $t_{\xi}$  and  $t_{\xi} + \Delta t_{\xi}$  with  $\Delta t_{\xi} < 0.38 \times t_{\xi}$ . The value of  $v_{\infty}$  was estimated by fitting a linear function to the values  $\left\langle \frac{\partial h_{\xi}}{\partial t_{\xi}} \right\rangle$  with respect to  $t_{\xi}^{-2/3}$  in the range  $(0, w)$  and taking the value of the intercept. The value of  $w$  varied from 0.15 to 0.2, and the overall uncertainty was derived from the combined statistical uncertainty ranges. We estimated the value of  $\Gamma$  by fitting a linear function to  $t_{\xi}^{-2/3} \langle h_{\xi}^2 \rangle_c$  versus  $t_{\xi}^{-2/3}$  in the range  $(0, w')$  and calculating  $(B/\langle \chi_1^2 \rangle_c)^{3/2}$ , where  $B$  is the intercept value and  $\chi_1$  is the random variable following the Gaussian orthogonal ensemble Tracy–Widom distribution [30]. The value of  $w'$  was varied from 0.15 to 0.2 (from 0.4 to 0.6) in the DP (CDP) models, respectively, and the overall uncertainty was derived from the combined statistical uncertainty ranges.

### Height spatial covariance

We observed a data collapse upon rescaling  $C_{s,int}(l, t_{\xi})$  and  $l$  by the APT dynamical correlation length in the short-time regime, and by the KPZ-class fluctuation amplitude and correlation length in the long-time regime. In the long-time limit, the values agreed with those of the exact solution for the KPZ class with flat initial conditions, the  $\text{Airy}_1$  covariance. The Langevin equations showed the same behavior as the discrete models (Figs. S21 and S22 [26]).

\* ysk@yfukai.net

- [1] H. Hinrichsen, Non-equilibrium critical phenomena and phase transitions into absorbing states, *Advances in Physics* **49**, 815 (2000).
- [2] M. Henkel, H. Hinrichsen, and S. Luebeck, *Non-Equilibrium Phase Transitions: Volume 1: Absorbing*

- Phase Transitions* (Springer, Dordrecht Netherlands ; New York, 2009).
- [3] K. A. Takeuchi, Experimental approaches to universal out-of-equilibrium scaling laws: turbulent liquid crystal and other developments, *Journal of Statistical Mechanics: Theory and Experiment* **2014**, P01006 (2014).
  - [4] A.-L. Barabási and H. E. Stanley, *Fractal Concepts in Surface Growth* (Cambridge University Press, 1995).
  - [5] I. Corwin, The Kardar–Parisi–Zhang Equation and Universality Class, *Random Matrices: Theory and Applications* **01**, 1130001 (2012).
  - [6] K. A. Takeuchi, An appetizer to modern developments on the Kardar–Parisi–Zhang universality class, *Physica A: Statistical Mechanics and its Applications* **504**, 77 (2018).
  - [7] K. Avila, D. Moxey, A. de Lozar, M. Avila, D. Barkley, and B. Hof, The Onset of Turbulence in Pipe Flow, *Science* **333**, 192 (2011).
  - [8] G. Lemoult, L. Shi, K. Avila, S. V. Jalikop, M. Avila, and B. Hof, Directed percolation phase transition to sustained turbulence in Couette flow, *Nature Physics* **12**, 254 (2016).
  - [9] M. Sano and K. Tamai, A universal transition to turbulence in channel flow, *Nature Physics* **12**, 249 (2016).
  - [10] T. E. Harris, Contact Interactions on a Lattice, *The Annals of Probability* **2**, 969 (1974).
  - [11] M. Eden, A Two-dimensional Growth Process, in *Proceedings of the Fourth Berkeley Symposium on Mathematical Statistics and Probability, Volume 4: Contributions to Biology and Problems of Medicine* (The Regents of the University of California, 1961).
  - [12] T. Williams and R. Bjerknes, Stochastic Model for Abnormal Clone Spread through Epithelial Basal Layer, *Nature* **236**, 19 (1972).
  - [13] J.-i. Wakita, H. Itoh, T. Matsuyama, and M. Matsushita, Self-Affinity for the Growing Interface of Bacterial Colonies, *Journal of the Physical Society of Japan* **66**, 67 (1997).
  - [14] S. F. Edwards and D. R. Wilkinson, The Surface Statistics of a Granular Aggregate, *Proceedings of the Royal Society of London A: Mathematical, Physical and Engineering Sciences* **381**, 17 (1982).
  - [15] M. Kardar, G. Parisi, and Y.-C. Zhang, Dynamic scaling of growing interfaces, *Physical Review Letters* **56**, 889 (1986).
  - [16] H. Kaya, A. Kabakçioğlu, and A. m. c. Erzan, Delocalization transition of a rough adsorption-reaction interface, *Phys. Rev. E* **61**, 1102 (2000).
  - [17] C. Mueller and R. Tribe, A phase transition for a stochastic PDE related to the contact process, *Probability Theory and Related Fields* **100**, 131 (1994).
  - [18] C. Mueller and R. B. Sowers, Random Travelling Waves for the KPP Equation with Noise, *Journal of Functional Analysis* **128**, 439 (1995).
  - [19] R. Tribe, A travelling wave solution to the kolmogorov equation with noise, *Stochastics and Stochastic Reports* **56**, 317 (1996).
  - [20] C. R. Doering, C. Mueller, and P. Smereka, Interacting particles, the stochastic Fisher–Kolmogorov–Petrovsky–Piscounov equation, and duality, *Physica A: Statistical Mechanics and its Applications Stochastic Systems: From Randomness to Complexity*, **325**, 243 (2003).
  - [21] L. Pechenik and H. Levine, Interfacial velocity corrections due to multiplicative noise, *Physical Review E* **59**, 3893 (1999).
  - [22] S. Nestic, R. Cuerno, and E. Moro, Macroscopic response to microscopic intrinsic noise in three-dimensional fisher fronts, *Phys. Rev. Lett.* **113**, 180602 (2014).
  - [23] E. Moro, Internal Fluctuations Effects on Fisher Waves, *Physical Review Letters* **87**, 238303 (2001).
  - [24] J. Wang, Z. Zhou, Q. Liu, T. M. Garoni, and Y. Deng, High-precision Monte Carlo study of directed percolation in (d+1) dimensions, *Physical Review E* **88**, 042102 (2013).
  - [25] E. Domany and W. Kinzel, Equivalence of Cellular Automata to Ising Models and Directed Percolation, *Physical Review Letters* **53**, 311 (1984).
  - [26] See End Matter and Supplemental Material for the detailed simulation and analysis methods, Tables AI–AIII, Tables SI–SVIII, and Figs. A1 and S1–S22, which includes Refs. [27, 39, 44, 45].
  - [27] I. Dornic, H. Chaté, and M. A. Muñoz, Integration of Langevin Equations with Multiplicative Noise and the Viability of Field Theories for Absorbing Phase Transitions, *Physical Review Letters* **94**, 100601 (2005).
  - [28] M. Prähofer and H. Spohn, Universal distributions for growth processes in 1 + 1 dimensions and random matrices, *Phys. Rev. Lett.* **84**, 4882 (2000).
  - [29] K. A. Takeuchi and M. Sano, Universal fluctuations of growing interfaces: Evidence in turbulent liquid crystals, *Phys. Rev. Lett.* **104**, 230601 (2010).
  - [30] K. A. Takeuchi and M. Sano, Evidence for Geometry-Dependent Universal Fluctuations of the Kardar–Parisi–Zhang Interfaces in Liquid-Crystal Turbulence, *Journal of Statistical Physics* **147**, 853 (2012).
  - [31] J. Krug, P. Meakin, and T. Halpin-Healy, Amplitude universality for driven interfaces and directed polymers in random media, *Physical Review A* **45**, 638 (1992).
  - [32] N. Caballero, E. Agoritsas, V. Lecomte, and T. Giamarchi, From bulk descriptions to emergent interfaces: Connecting the Ginzburg–Landau and elastic-line models, *Physical Review B* **102**, 104204 (2020).
  - [33] O. Hallatschek and K. S. Korolev, Fisher Waves in the Strong Noise Limit, *Physical Review Letters* **103**, 108103 (2009).
  - [34] Y. T. Fukai and K. A. Takeuchi, Kardar–Parisi–Zhang Interfaces with Curved Initial Shapes and Variational Formula, *Physical Review Letters* **124**, 060601 (2020).
  - [35] K. A. Takeuchi, M. Kuroda, H. Chaté, and M. Sano, Directed Percolation Criticality in Turbulent Liquid Crystals, *Physical Review Letters* **99**, 234503 (2007).
  - [36] K. R. Mesa, K. Kawaguchi, K. Cockburn, D. Gonzalez, J. Boucher, T. Xin, A. M. Klein, and V. Greco, Homeostatic Epidermal Stem Cell Self-Renewal Is Driven by Local Differentiation, *Cell Stem Cell* **23**, 677 (2018).
  - [37] K. A. Takeuchi, M. Kuroda, H. Chaté, and M. Sano, Experimental realization of directed percolation criticality in turbulent liquid crystals, *Physical Review E* **80**, 051116 (2009).
  - [38] Theoretical curves available in the following URL were used: <https://www-m5.ma.tum.de/KPZ>.
  - [39] F. Bornemann, On the numerical evaluation of fredholm determinants, *Math. Comput.* **79**, 871 (2010).
  - [40] Precisely,  $k = \sum_{i', j' \in I} \rho((i', j'), t)$ ,  $I = \{(i, j), (i + \sigma, j), (i, j + \sigma), (i + \sigma, j + \sigma)\}$  and  $\sigma = 1$

- ( $\sigma = -1$ ) for the odd (even) timesteps, respectively.
- [41] H.-K. Janssen, Survival and percolation probabilities in the field theory of growth models, *Journal of Physics: Condensed Matter* **17**, S1973 (2005).
  - [42] T. Shimaya and K. A. Takeuchi, Lane formation and critical coarsening in a model of bacterial competition, *Physical Review E* **99**, 042403 (2019).
  - [43] P. L. Krapivsky, Kinetics of monomer-monomer surface catalytic reactions, *Physical Review A* **45**, 1067 (1992).
  - [44] W. H. Press, S. A. Teukolsky, W. T. Vetterling, and B. P. Flannery, *Numerical Recipes 3rd Edition: The Art of Scientific Computing*, 3rd ed. (Cambridge University Press, Cambridge, UK ; New York, 2007).
  - [45] M. Newville, R. Otten, A. Nelson, T. Stensitzki, A. Ingargiola, D. Allan, A. Fox, F. Carter, Michał, R. Osborn, D. Pustakhod, S. Weigand, Ineuhaus, A. Aristov, Glenn, Mark, mgunyho, C. Deil, A. L. R. Hansen, G. Pasquevich, L. Foks, N. Zobrist, O. Frost, Stuermer, J.-C. Jaskula, S. Caldwell, P. Eendebak, M. Pompili, J. H. Nielsen, and A. Persaud, *Lmfit/lmfit-py: 1.3.1*, Zenodo (2024).

# Supplementary material for Universal interface fluctuations in absorbing-state phase transitions

Yohsuke T. Fukai,<sup>1,2,3,\*</sup> Keiichi Tamai,<sup>3,4,5</sup> and Tetsuya Hiraiwa<sup>3,6,7,8,9</sup>

<sup>1</sup>*Nonequilibrium Physics of Living Matter Laboratory, RIKEN Pioneering Research Institute, 2-2-3 Minatojima-minamimachi, Chuo-ku, Kobe, Hyogo 650-0047, Japan*

<sup>2</sup>*Nonequilibrium Physics of Living Matter Riken Hakubi Research Team, RIKEN Center for Biosystems Dynamics Research, 2-2-3 Minatojima-minamimachi, Chuo-ku, Kobe, Hyogo 650-0047, Japan*

<sup>3</sup>*Department of Physics, The University of Tokyo, 7-3-1 Hongo, Bunkyo-ku, Tokyo 113-0033, Japan*

<sup>4</sup>*Institute for Physics of Intelligence, The University of Tokyo, 7-3-1 Hongo, Bunkyo-ku, Tokyo 113-0033, Japan*

<sup>5</sup>*The Institute for Solid State Physics, The University of Tokyo, 5-1-5 Kashiwanoha, Kashiwa, Chiba 277-8581, Japan*

<sup>6</sup>*Institute of Physics, Academia Sinica, No. 128, Section 2, Academia Road, Taipei 11529, Taiwan*

<sup>7</sup>*Physics Division, National Center for Theoretical Sciences, Taipei 106319, Taiwan*

<sup>8</sup>*Mechanobiology Institute, National University of Singapore, 5A Engineering Drive 1, Singapore 117411, Singapore*

<sup>9</sup>*Universal Biology Institute, The University of Tokyo, 7-3-1 Hongo, Bunkyo-ku, Tokyo 113-0033, Japan*

(Dated: May 20, 2026)

## SUPPLEMENTARY TEXT 1: DOMANY-KINZEL MODEL AND BIASED VOTER MODEL

We implemented a parallel-update biased voter model as a variant of the Domany-Kinzel (DK) model as follows. We considered two square lattices arranged in a checkerboard pattern (white and gray sites in Fig. S1). In each timestep, we alternately selected the sites on one of the two lattices and updated each site's state to that of a stochastically chosen nearest-neighbor site on the other lattice. We set the probabilities of choosing an active and an inactive site,  $p_+$  and  $p_-$ , respectively, so that they satisfy  $p_+ : p_- = (1 + \frac{\epsilon}{2}) : (1 - \frac{\epsilon}{2})$ , thus

$$p_{\pm} = \frac{2 \pm \epsilon}{8 + 2\epsilon(k - 2)}, \quad (\text{S1})$$

where  $k$  is the number of nearest-neighbor active sites. In terms of the Domany-Kinzel model, this corresponds to choosing  $p_k$  to be

$$p_k = \frac{(2 + \epsilon)k}{8 + 2\epsilon(k - 2)}. \quad (\text{S2})$$

## SUPPLEMENTARY TEXT 2: NUMERICAL SIMULATION OF LANGEVIN EQUATIONS

We simulated the Langevin equation

$$\frac{\partial \rho(\mathbf{x}, t)}{\partial t} = D\Delta\rho + A\rho - B\rho^2 + \sigma\sqrt{f(\rho)}\eta(\mathbf{x}, t) \quad (\text{1})$$

using the scheme of Ref. [S1] summarized as follows. First, we approximated the spatial derivative by finite differences to obtain

$$\frac{d}{dt}\rho_{i,j}(t) = D\Delta\rho_{i,j} + A\rho_{i,j} - B\rho_{i,j}^2 + \frac{\sigma}{\Delta x}\sqrt{f(\rho_{i,j})}\eta_{i,j}(t) \quad (\text{S3})$$

where

$$\rho_{i,j}(t) := \rho(i\Delta x, j\Delta x, t), \quad (\text{S4})$$

$$\Delta\rho_{i,j}(t) := \alpha_{i,j} - \frac{4\rho_{i,j}(t)}{(\Delta x)^2}, \quad (\text{S5})$$

$$\alpha_{i,j} := (\Delta x)^{-2} \sum_{\substack{k=-1,1 \\ l=-1,1}} \rho_{i+k,j+l}(t) \quad (\text{S6})$$

and  $\eta_{i,j}(t)$  is a white Gaussian noise satisfying  $\langle \eta_{i,j}(t) \rangle = 0$ ,  $\langle \eta_{i',j'}(t') \eta_{i,j}(t) \rangle = \delta_{i',i} \delta_{j',j} \delta(t' - t)$ . The prefactor  $\frac{1}{\Delta x}$  in the last term is chosen so that the stochastic term has the same distribution as the spatially averaged noise term of the continuous version,  $\frac{1}{(\Delta x)^2} \int_x^{x+\Delta x} dx' \int_y^{y+\Delta x} dy' \eta(x', y', t)$ .

Regarding the time discretization, it is known that a naïve Euler-type scheme, which approximates the noise term by a Gaussian random variable, is inappropriate because it can violate the non-negativity condition  $\rho(x, y, t) \geq 0$ , a crucial property of the solution of the directed percolation (DP) Langevin equation.

To avoid this problem, we used the scheme proposed in Ref. [S1], which is an operator splitting method [S2] that splits the terms into groups, each of which can be treated exactly, and integrates the terms group by group. The steps for a single timestep  $\Delta t$  are as follows:

1. In Eq. (S3), we first integrate the terms  $D\Delta\rho_{i,j} + A\rho_{i,j} + \frac{\sigma}{\Delta x} \sqrt{f(\rho_{i,j})} \eta_{i,j}(t)$  by integrating the stochastic differential equation (SDE)

$$\frac{d}{dt} \rho(t) = \beta\rho + \tilde{\alpha} + \tilde{\sigma} \sqrt{f(\rho)} \eta_{i,j}(t) \quad (\text{S7})$$

with the initial condition  $\rho(0) = \rho_{i,j}(t)$  for the timestep  $\Delta t$ , where  $\tilde{\alpha} := D\alpha_{i,j}$  is treated as a constant,  $\tilde{\sigma} := \frac{\sigma}{\Delta x}$ , and  $\beta := A - \frac{4D}{(\Delta x)^2}$ .

- For the DP Langevin equation ( $f(\rho) = \rho$ ), this step is conducted by using the exact solution for the Fokker-Plank equation of the SDE [Eq. (S7)], which leads to the expression for  $\rho^* := \rho(\Delta t)$  [S1]:

$$\rho^* = \text{Gamma}[\mu + 1 + \text{Poisson}[\lambda\omega\rho(0)]] / \lambda \quad (\text{S8})$$

where  $\text{Gamma}[z]$  is a random variable following the gamma distribution with the shape parameter  $z$  and the scale parameter 1,  $\text{Poisson}[w]$  is a random variable following the Poisson distribution with the mean  $w$ ,  $\mu := -1 + \frac{2\tilde{\alpha}}{\tilde{\sigma}^2} = -1 + \frac{2D\alpha_{i,j}(\Delta x)^2}{\sigma^2}$ ,  $\lambda := \frac{2\beta}{\tilde{\sigma}^2(\omega-1)} = \frac{2\beta(\Delta x)^2}{\sigma^2(\omega-1)}$  and  $\omega := e^{\beta t}$ .

- For the compact directed percolation (CDP) Langevin equation ( $f(\rho) = \rho(1 - \rho)$ ), we approximate the term  $\sqrt{\rho(1 - \rho)}$  by

$$\begin{cases} \sqrt{\rho} & (\rho < \frac{1}{2}) \\ \sqrt{1 - \rho} & (\rho > \frac{1}{2}), \end{cases} \quad (\text{S9})$$

following [S1], and use the same scheme as the DP case. If  $\rho$  exactly equals  $\frac{1}{2}$  within the numerical precision, either branch of Eq. (S9) is chosen randomly.

2. We then integrate the remaining part  $-B\rho_{i,j}^2$  for the timestep  $\Delta t$  by solving  $d_t\rho(t) = -B\rho^2$  with the initial condition  $\rho(0) = \rho^*$  to obtain

$$\rho_{i,j}(t + \Delta t) = \rho(\Delta t) = \frac{\rho^*}{1 + \rho^* B \Delta t}. \quad (\text{S10})$$

It has been shown that this algorithm preserves the non-negativity of the solution [S1].

### Supplementary Text 3: Details of nonuniversal parameter estimation

#### Stationary density of the DP models

To estimate  $\rho_\infty(\epsilon)$  for the DP models, we defined a timescale  $t_{\text{stat}}$  substantially longer than the correlation time, and then calculated the average of  $\rho(\mathbf{x}, t)$  for  $t > t_{\text{stat}}$ , which we denote by  $\langle \rho(\mathbf{x}, t) \rangle_{t > t_{\text{stat}}}$ . We varied  $t_{\text{stat}}$  from  $10 \times \xi_{\parallel}(\epsilon)$

to  $20 \times \xi_{\parallel}(\epsilon)$ , deriving the overall uncertainty by combining the statistical uncertainty ranges ( $2 \times$  standard error) over these intervals.

For the bond percolation model, we averaged the values of  $\tilde{\rho}$  for  $\epsilon \leq 0.01$  to estimate  $\rho_{\infty}$ . For the DP Langevin equation, we empirically fitted a linear function to the values. The estimated parameters are summarized in Table SVI.

*Characteristic length scale of the DP models*

To estimate the characteristic length  $x_0$  for the DP models, we fitted the empirical function  $A\tilde{l}^{-\beta^{\text{DP}}/\nu_{\perp}^{\text{DP}}} e^{-\tilde{l}/x_0}$  to the values of  $C_s(l, t = t_{\text{max}})/\rho_{\infty}(\epsilon)^2$ , where  $\tilde{l} := l/\epsilon^{-\nu_{\perp}^{\text{DP}}}$ ,  $A$  is a model-dependent constant, and  $t_{\text{max}}$  is the maximum  $t$  value indicated in Table SI. The fitting was performed by the Levenberg-Marquardt algorithm [`scipy.optimize.curve_fit` function in the `scipy` package (version 1.10.1)] with the initial guess  $A = 0.03$  and  $x_0 = 1$  and the maximum function evaluation `maxfev=1000000`. The universal parameter  $C_{s0} = Ax_0^{\beta/\nu_{\perp}}$  was estimated to be 0.61(7). The estimated parameters are summarized in Table SVI, and the fitted function is shown in Fig. S7.

**SUPPLEMENTAL TABLES**

TABLE SI: (Attached as a separate file.) Parameters for the quench simulations of the DP-class models for Figs. S2, S3, and S7. All simulations of the directed percolation were conducted with  $L_x = L_y = 16384$ . All simulations of the Langevin equation were conducted with  $L_x = L_y = 8192$ ,  $D = 1$ , and  $\sigma = 1$ . All simulations were conducted with the double-precision float.

TABLE SII: (Attached as a separate file.) Parameters for the quench simulations of the CDP-class models for Figs. S4, S5, S6. All simulations of the biased voter model and Langevin equation were conducted with  $L_x = L_y = 32768$  and  $L_x = L_y = 8192$ , respectively, with the double-precision float.

TABLE SIII: (Attached as a separate file.) The parameters for the quench simulations of the CDP-class models at criticality ( $\epsilon = 0$ ) for Figs. S8 and S9. All simulations of the biased voter model and Langevin equation were conducted with  $L_x = L_y = 16384$  and  $L_x = L_y = 8192$ , respectively, with the double-precision float.

TABLE SIV: (Attached as a separate file) Parameters for the simulation of DP-class models with the active wall. All Langevin simulations were conducted with  $D = 1$  and  $\sigma = 1$  with the single-precision float.

TABLE SV: (Attached as a separate file) Parameters for the simulation of CDP-class models with the active wall. All Langevin simulations were conducted with  $\rho_b = 1$  with the single-precision float.

TABLE SVI: Estimated nonuniversal parameters for the DP models. The uncertainties were derived by combining uncertainty ranges of the fitting parameters estimated for different fitting ranges, estimated values of the critical parameter, and the exponent values.

name	$t_0$	$\rho_0$	$x_0$
Bond percolation	0.463(6)	1.642(5)	0.21(1)
DP Langevin	6.97(5)	0.1684(5) + 0.17(1) $\epsilon$	1.71(8)

TABLE SVII: Estimated nonuniversal parameters for the CDP models. The values of  $t'_0$  were omitted due to their large uncertainties. The uncertainties were derived by combining the uncertainties of the fitting parameters estimated for different fitting ranges.

model	$D$	$\sigma$	$C_1$	$C_2$	$D'$	$C_{\text{dyn}}$
Biased voter	–	–	0.66(2)	0.150(3)	2.13(5)	0.18(6)
CDP Langevin	0.1	1	1.3(4)	0.54(4)	0.85(1)	0.21(4)
	0.25	0.5	1.0(1)	0.07(2)	2.03(2)	0.10(1)
	0.25	1	1.3(3)	0.22(4)	2.09(2)	0.16(3)
	0.25	2	1.7(7)	1.1(1)	2.05(5)	0.19(9)
	0.5	1	1.2(1)	0.13(2)	4.0(3)	0.13(4)
	0.5	1.414214	1.2(3)	0.29(5)	4.0(1)	0.15(9)
	1	1	1.13(9)	0.07(1)	7.7(1)	0.10(3)
	2	1	1.14(7)	0.04(1)	14.5(5)	0.080(4)

TABLE SVIII: Estimated parameters of the KPZ class in the long-time regime (full table). The meaning of the column values is denoted in the caption of AIII. The values are also shown in Fig. S18.

model	$D$	$\sigma$	$\rho_b$	$v_\infty$			$\Gamma$		
				Value	Max	Min	Value	Max	Min
Bond percolation	–	–	–	2.756(3)	2.894	2.627	14.2(1)	16.8	12.1
DP Langevin	1	1	0.1	2.84(1)	3.00	2.70	15.1(5)	18.5	12.5
			1	2.83(1)	2.99	2.68	16(1)	21	12
			10	2.825(3)	2.968	2.694	15.6(4)	18.8	12.9
Biased voter	–	–	–	0.540(3)	0.556	0.524	0.132(3)	0.149	0.121
CDP Langevin	0.1	1	1	0.535(1)	0.561	0.510	0.146(3)	0.179	0.125
	0.25	0.5	1	0.5865(3)	0.6207	0.5543	0.088(2)	0.108	0.068
		1	1	0.5471(4)	0.5906	0.5090	0.124(3)	0.169	0.092
		2	1	0.560(4)	0.606	0.519	0.149(3)	0.198	0.119
	0.5	1	1	0.573(3)	0.616	0.537	0.102(2)	0.128	0.083
		1.414214	1	0.579(8)	0.655	0.521	0.128(2)	0.170	0.095
	1	1	1	0.592(3)	0.623	0.557	0.089(3)	0.106	0.070
	2	1	1	0.615(1)	0.648	0.588	0.069(3)	0.086	0.054

## SUPPLEMENTAL FIGURES

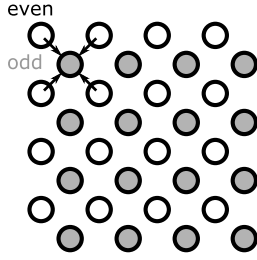


FIG. S1: An illustration of the lattice configuration of the two-dimensional Domany-Kinzel model. The white and gray circles indicate the lattice sites updated at the odd and even timesteps, respectively. The top-left site corresponds to  $(i, j) = (0, 0)$  for both lattices. The arrows indicate the four nearest-neighbor sites that contribute to the center site (see main text). Periodic boundary conditions are omitted from the illustration.

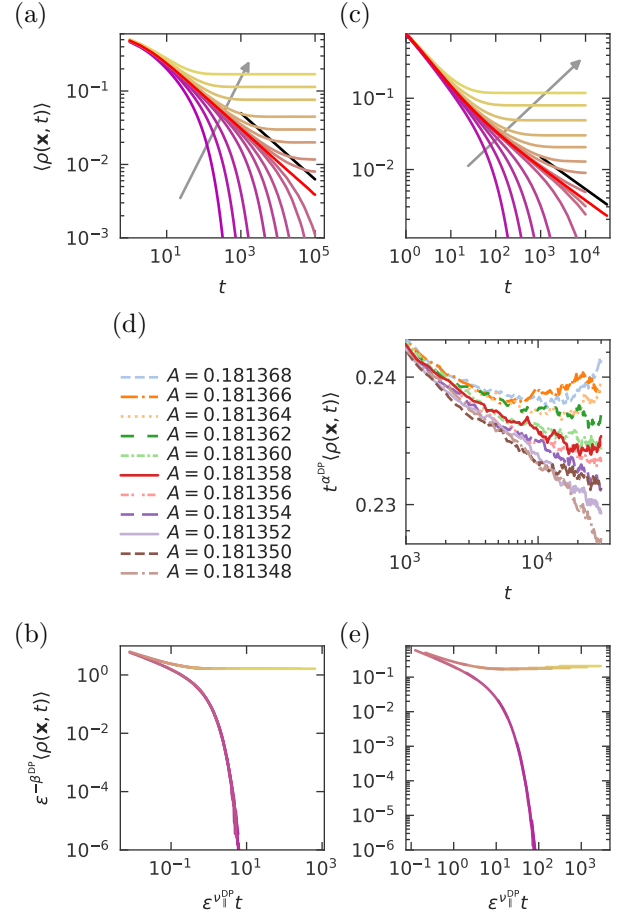


FIG. S2: The mean value of  $\rho(\mathbf{x}, t)$  for the quench simulations of (a,b) the bond percolation model and (c-e) the DP Langevin equation. (a,c) The original values  $\langle \rho(\mathbf{x}, t) \rangle$  against time  $t$ . Each line corresponds to a simulation with the control parameter listed in Table SI. The gray arrow indicates the direction in which the control parameter increases. The black line is a guide for the eye with the exponent  $t^{-\alpha^{\text{DP}}}$ , where  $\alpha^{\text{DP}} = \beta^{\text{DP}}/\nu_{\parallel}^{\text{DP}}$ . (d) The values rescaled to compensate for the expected power law  $t^{-\alpha^{\text{DP}}}$ . The control parameter values are shown in the legend. All simulations used 40 independent samples,  $D = 1$ ,  $\sigma = 1$ , and  $L_x = L_y = 8192$ . The critical point and its uncertainty were estimated by identifying the parameter range over which the values do not significantly increase or decrease. (b,e) Scaling collapse using the estimated transition-point values. The colors are the same as those used in (a,d).

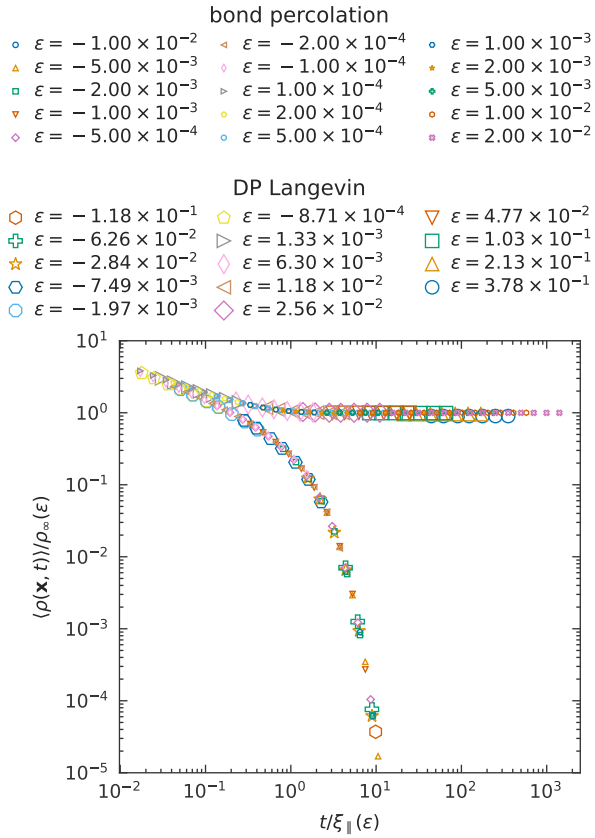


FIG. S3: The scaling collapse plot for the mean  $\rho(\mathbf{x}, t)$  for the quench simulations of the DP models.

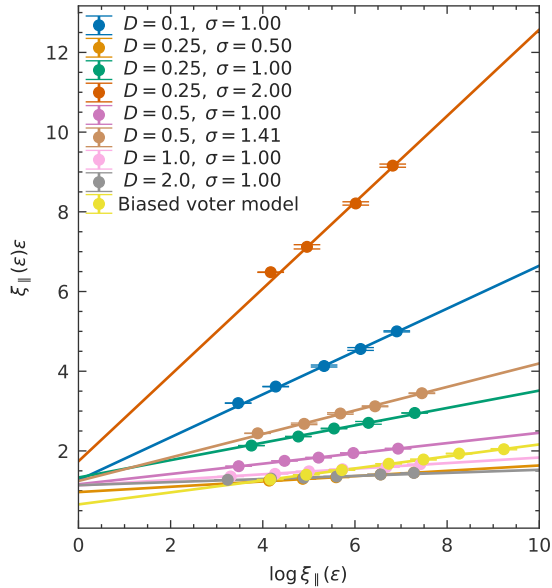


FIG. S4: Estimation of the correlation time  $\xi_{\parallel}(\varepsilon)$  for the CDP-class models. The lines are linear fits. The error bars indicate the overall uncertainty in the estimation of  $\xi_{\parallel}(\varepsilon)$ .

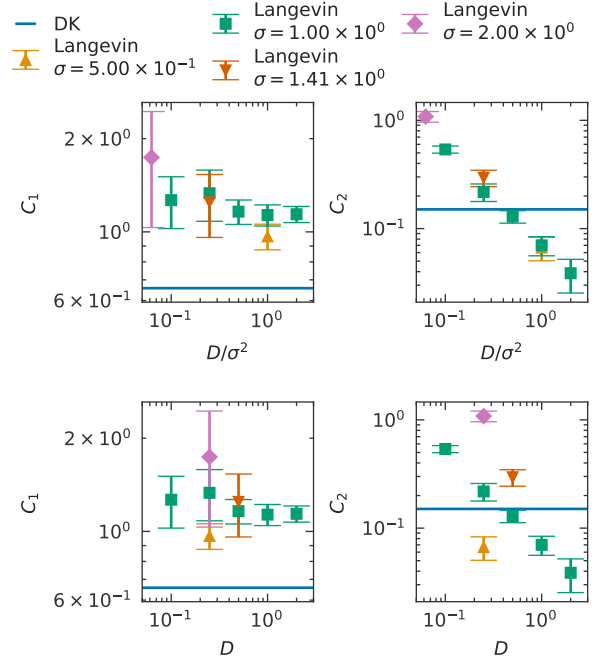


FIG. S5: The estimated parameters for the CDP correlation time plotted against  $D/\sigma^2$  and  $D$ . The points and error bars indicate the estimated values and uncertainties for the CDP Langevin equation, respectively. The blue horizontal solid line and shaded area indicate the value and uncertainty estimated for the DK model, respectively.

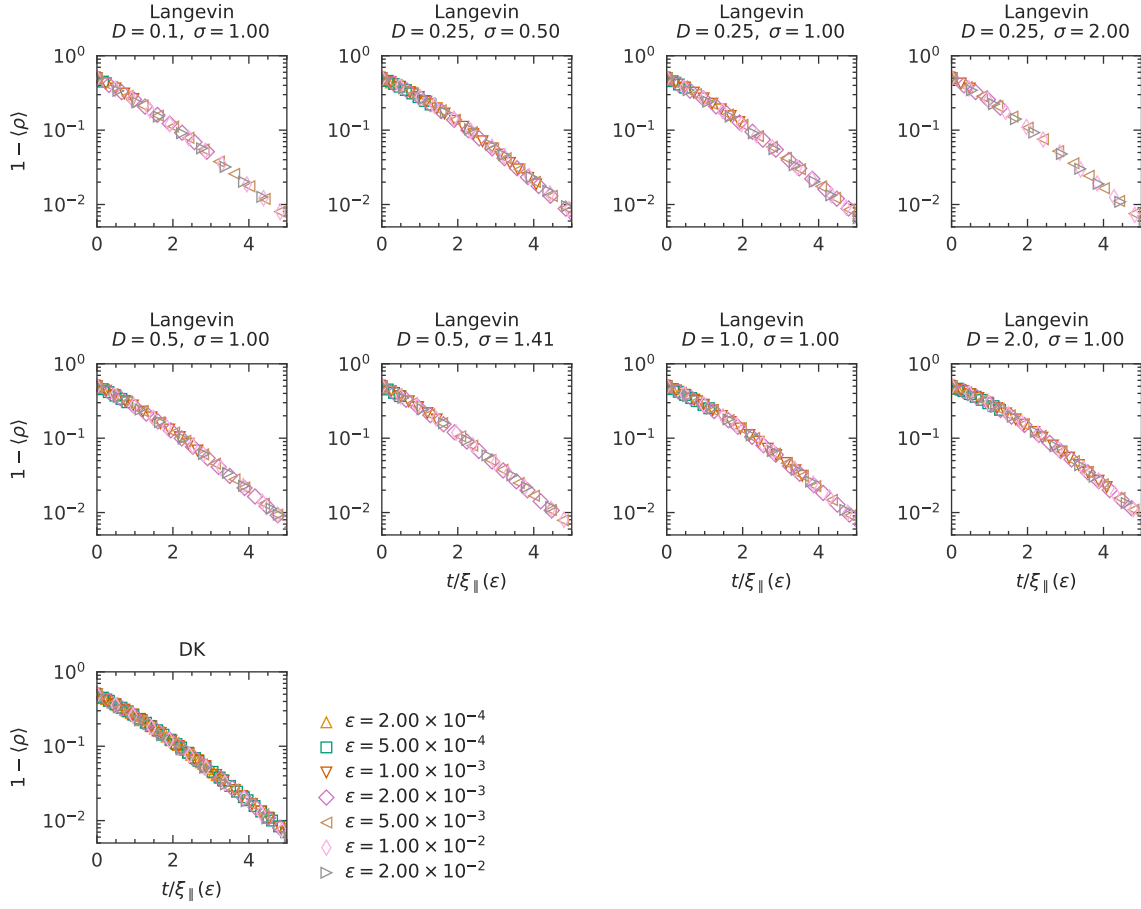


FIG. S6: The scaling collapse plot for the mean  $\rho(\mathbf{x}, t)$  for the quench simulations of CDP-class models.

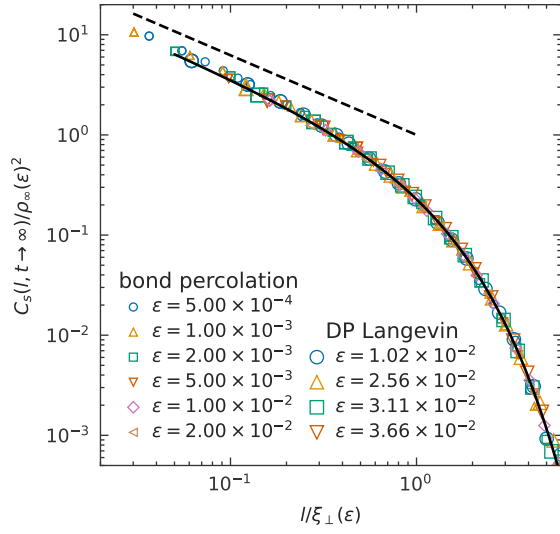


FIG. S7: The scaling collapse plot for the spatial covariance  $C_s(l, t)$  of the DP-class models for the stationary timescale  $t \gg \xi_{\parallel}(\epsilon)$ . The black solid line indicates the fitted spatial covariance function  $\tilde{C}(l/\xi_{\perp}(\epsilon))$ . The black dashed line is a guide for the eye with the exponent  $l^{-\beta^{\text{DP}}/\nu_{\perp}^{\text{DP}}}$ .

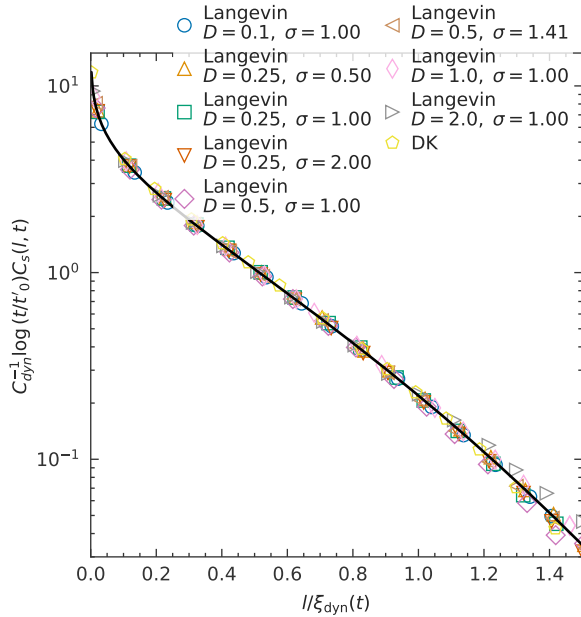


FIG. S8: The scaling collapse plot for the spatial covariance  $C_s(l, t)$  of the CDP-class models at criticality  $\epsilon = 0$ . The black solid lines indicate the exact function  $\text{Ei}_1 \left[ (l/\xi_{\text{dyn}}(\epsilon))^2 \right]$ .

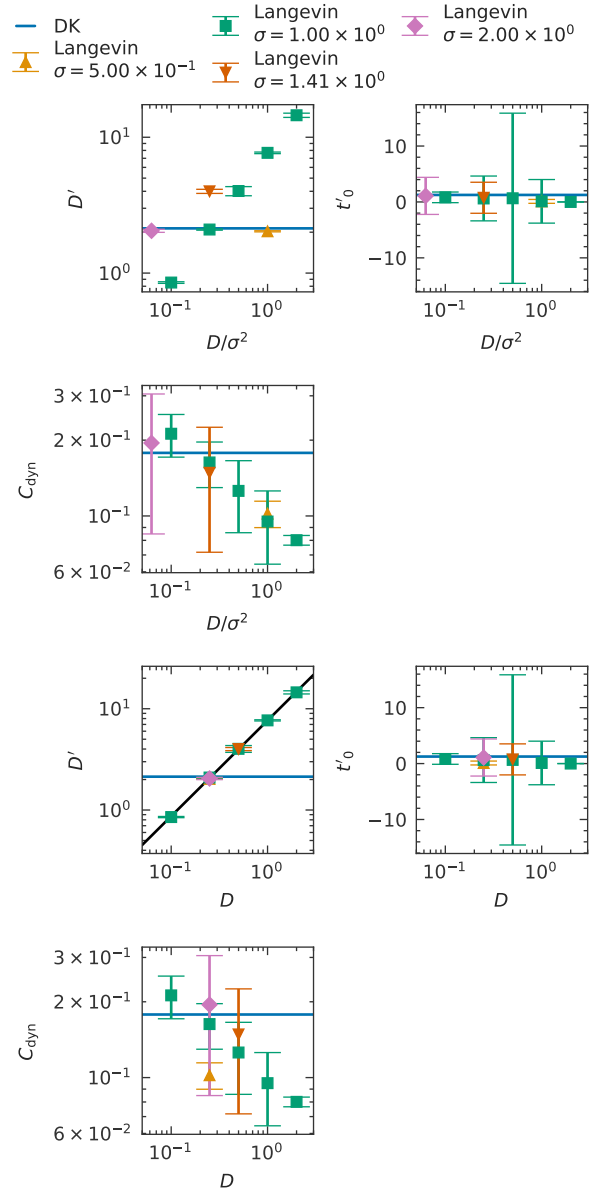


FIG. S9: The estimated parameters for the dynamical correlation length for the CDP-class models, plotted against  $D/b$  and  $D$ . The blue horizontal solid line and shaded area indicate the value and uncertainty estimated for the DK model, respectively. The black line in the plot of  $D'$  against  $D$  is the result of the linear fit on a log scale,  $D' = 7.7(1) \times D^{0.95(2)}$ .

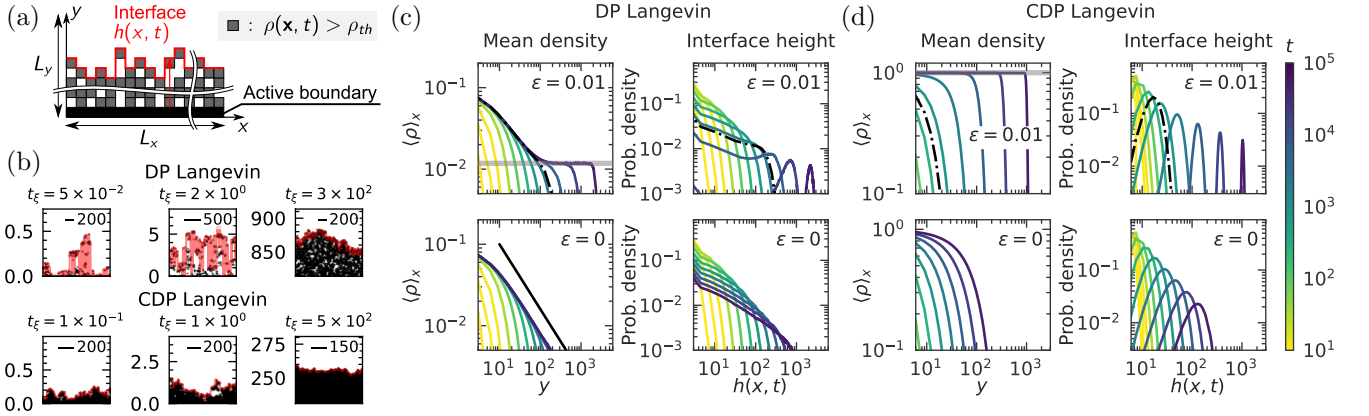


FIG. S10: Schematic and qualitative illustration of the interface growth process in the Langevin equation. (a) An illustration of the height definition with the active boundary. (b) Example snapshots of the active sites and the interface (red line) for the DP (upper) and CDP (lower) Langevin equations. The axis label and scale bar indicate the length rescaled by the correlation length  $\xi_\perp(\epsilon)$  and the actual length, respectively. The values of  $\epsilon$  and the rescaled time  $t_\xi = t/\xi_\parallel(\epsilon)$  are indicated in each plot. (c,d) The spanwise-averaged density  $\langle \rho(\mathbf{x}, t) \rangle_x$  (left) and the height probability distribution (right) for the DP (c) and CDP (d) Langevin equations. The top and bottom plots are the off-critical and critical cases, respectively. The dash-dot lines show the data at the correlation time  $t \approx \xi_\parallel(\epsilon)$ . The gray lines in the off-critical mean-density plots indicate  $\rho_\infty(\epsilon)$  (DP) and 1 (CDP). The black line in the inset of the left plot is a guide for the eye for the power law  $\langle \rho(\mathbf{x}, t) \rangle_x \propto y^{-\beta^{DP}/\nu_\perp}$ . For (b–d), parameters are set to  $D = \sigma = 1$ ,  $\rho_b = 0.1$ , and  $\rho_{th} = 0.1$  for the DP model, and  $D = 0.1$ ,  $\sigma = 1.0$ ,  $\rho_b = 1$ , and  $\rho_{th} = 0$  for the CDP model. The other parameters are summarized in Tables SIV and SV.

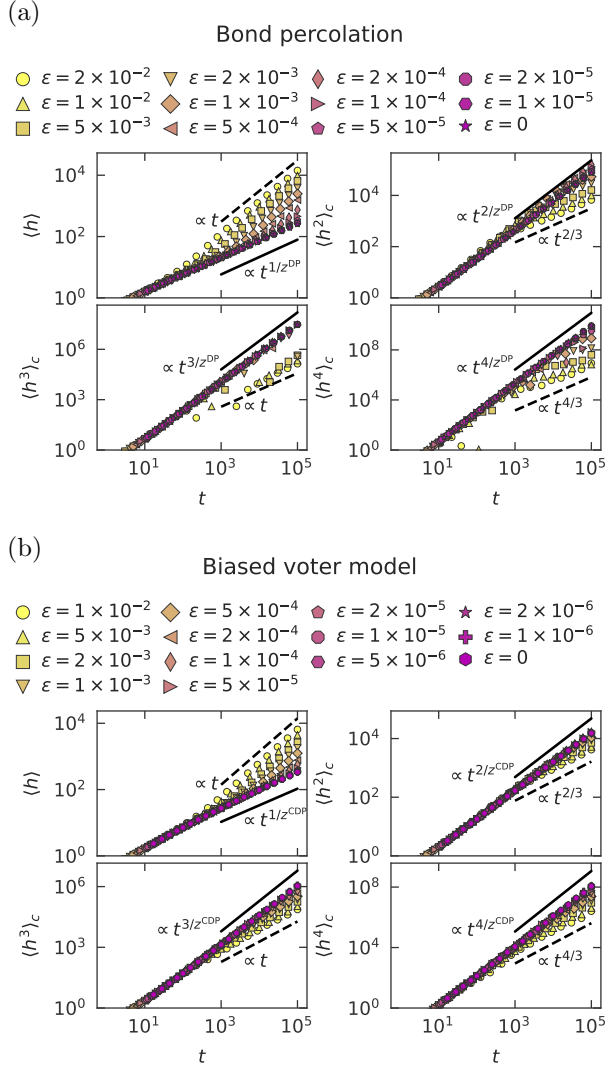


FIG. S11: Cumulants of the height distribution  $\langle h_\xi^k \rangle_c$  ( $k = 1, 2, 3, 4$ ) plotted against the raw time  $t$  for the (a) bond percolation and (b) biased voter models. The solid and dashed lines are guides for the eye for the APT and KPZ exponents, respectively (see the main text).

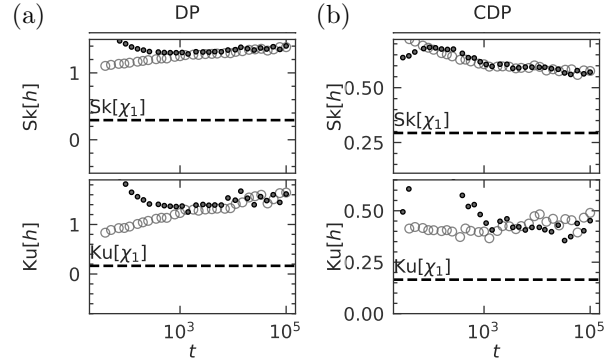


FIG. S12: Cumulant ratios of the height distribution for the (a) DP- and (b) CDP-class models. The plots show the skewness  $Sk[h]$  and the kurtosis  $Ku[h]$  for the critical cases. The larger unfilled and smaller filled symbols are for the discrete models and the Langevin equations ( $\rho_b = 0.1$  and  $\rho_{th} = 0.1$  for the DP Langevin equation, and  $\rho_{th} = 0$ ,  $D = 0.1$ ,  $\sigma = 1.0$  for the CDP Langevin equation), respectively. The dashed lines show the theoretical values for the GOE-TW distribution,  $\chi_1$ .

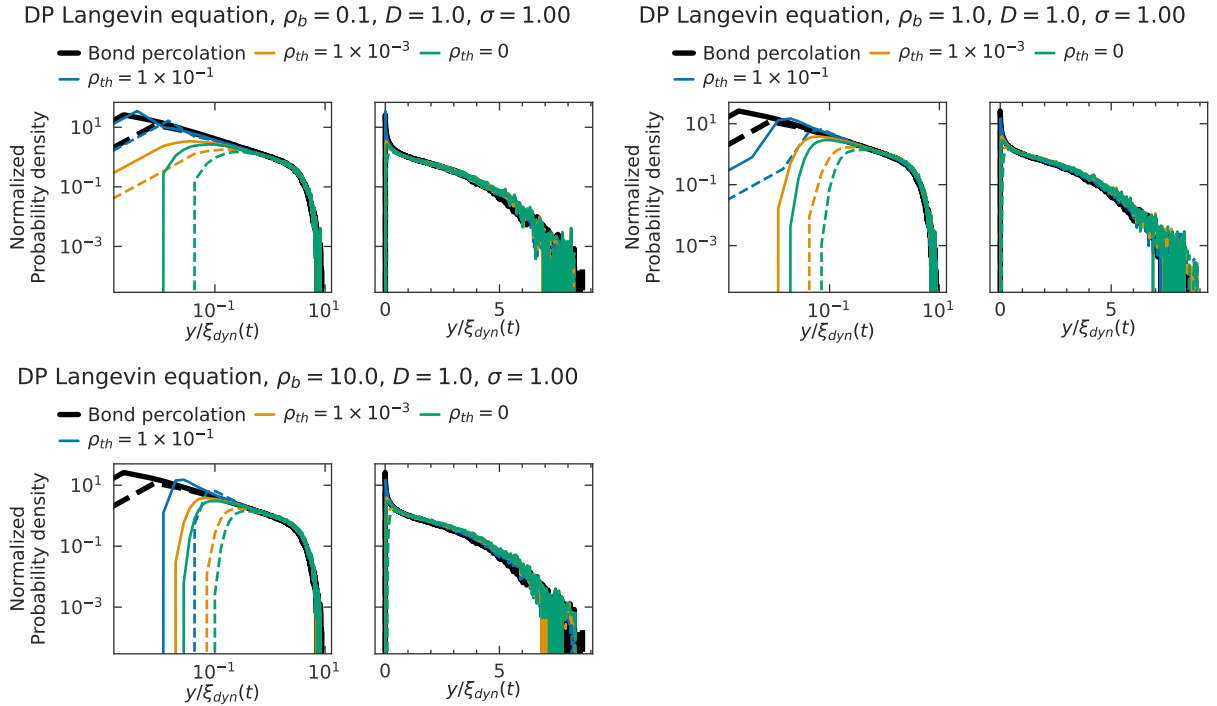


FIG. S13: The height distributions for the DP-class models at criticality ( $\epsilon = 0$ ), plotted with different  $\rho_b$ ,  $\rho_{th}$  and  $t$ . The dashed and solid lines show the data at  $t = 1 \times 10^4$  and  $t = 1 \times 10^5$ , respectively.



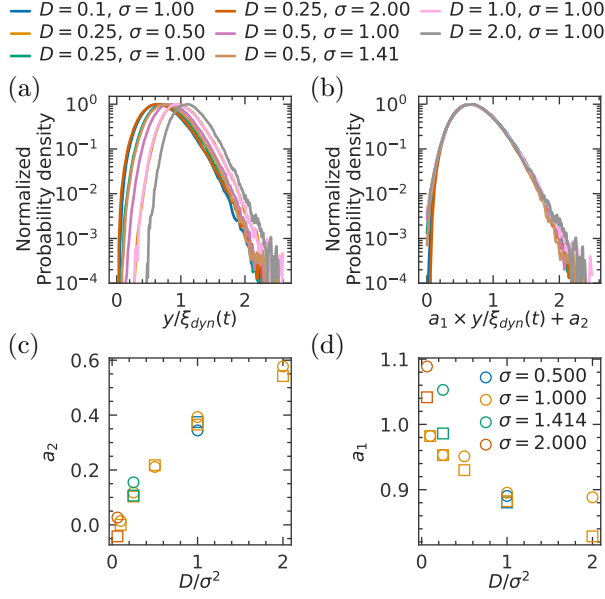


FIG. S15: (a) Height distributions for the CDP-class models at criticality ( $\epsilon = 0$ ) with  $\rho_{th} = 0$ , normalized to unity at the peak. (b) The same data as in (a), shifted by  $a_1$  and scaled by  $a_2$ , where  $a_1$  and  $a_2$  were estimated by minimizing the squared error with respect to the histogram of the DK model using the Nelder-Mead method via the `lmfit` package [S3]. (c,d) The estimated values of  $a_1$  and  $a_2$  plotted against  $D/\sigma^2$ . Squares and circles correspond to  $t = 1 \times 10^4$  and  $t = 1 \times 10^5$ , respectively.

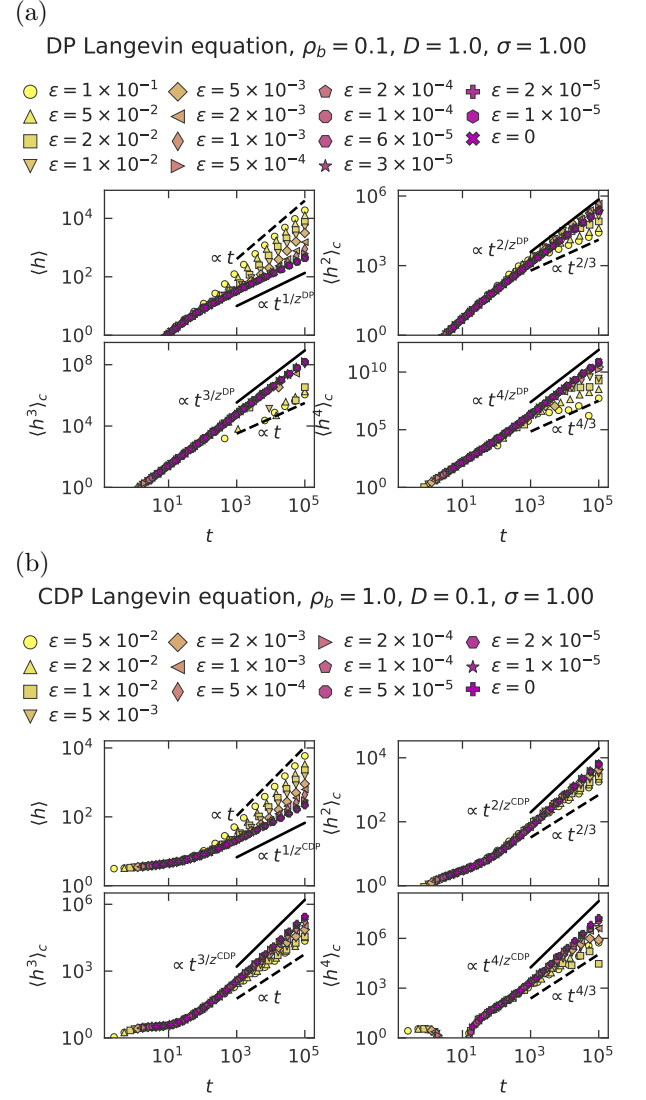


FIG. S16: Cumulants of the height distribution  $\langle h_\xi^k \rangle_c$  ( $k = 1, 2, 3, 4$ ) plotted against the raw time  $t$  for the (a) DP and (b) CDP Langevin equations. The solid and dashed lines are guides for the eye for the APT and KPZ exponents, respectively (see the main text). Parameters are set to  $D = \sigma = 1$ ,  $\rho_b = 0.1$ , and  $\rho_{th} = 0.1$  for the DP model, and  $D = 0.1$ ,  $\sigma = 1.0$ ,  $\rho_b = 1$ , and  $\rho_{th} = 0$  for the CDP model. The other parameters are summarized in Tables SIV and SV.

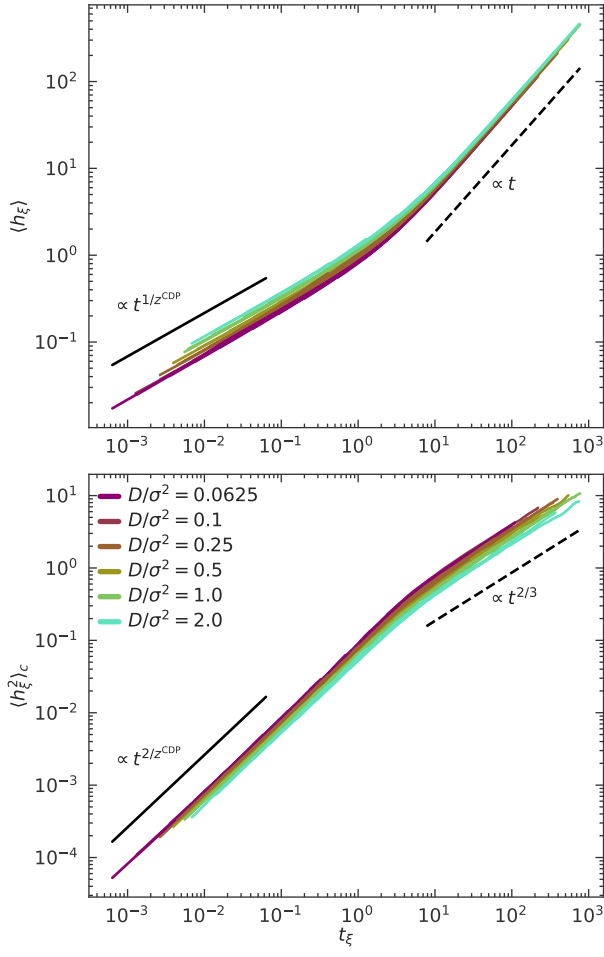


FIG. S17: First and second cumulants of the height distribution for the CDP-class models. Data with  $\rho_b = 1.0$  and  $\epsilon \leq 0.01$  are plotted. The solid and dashed lines are guides for the eye for the APT and KPZ exponents (see the main text), respectively.

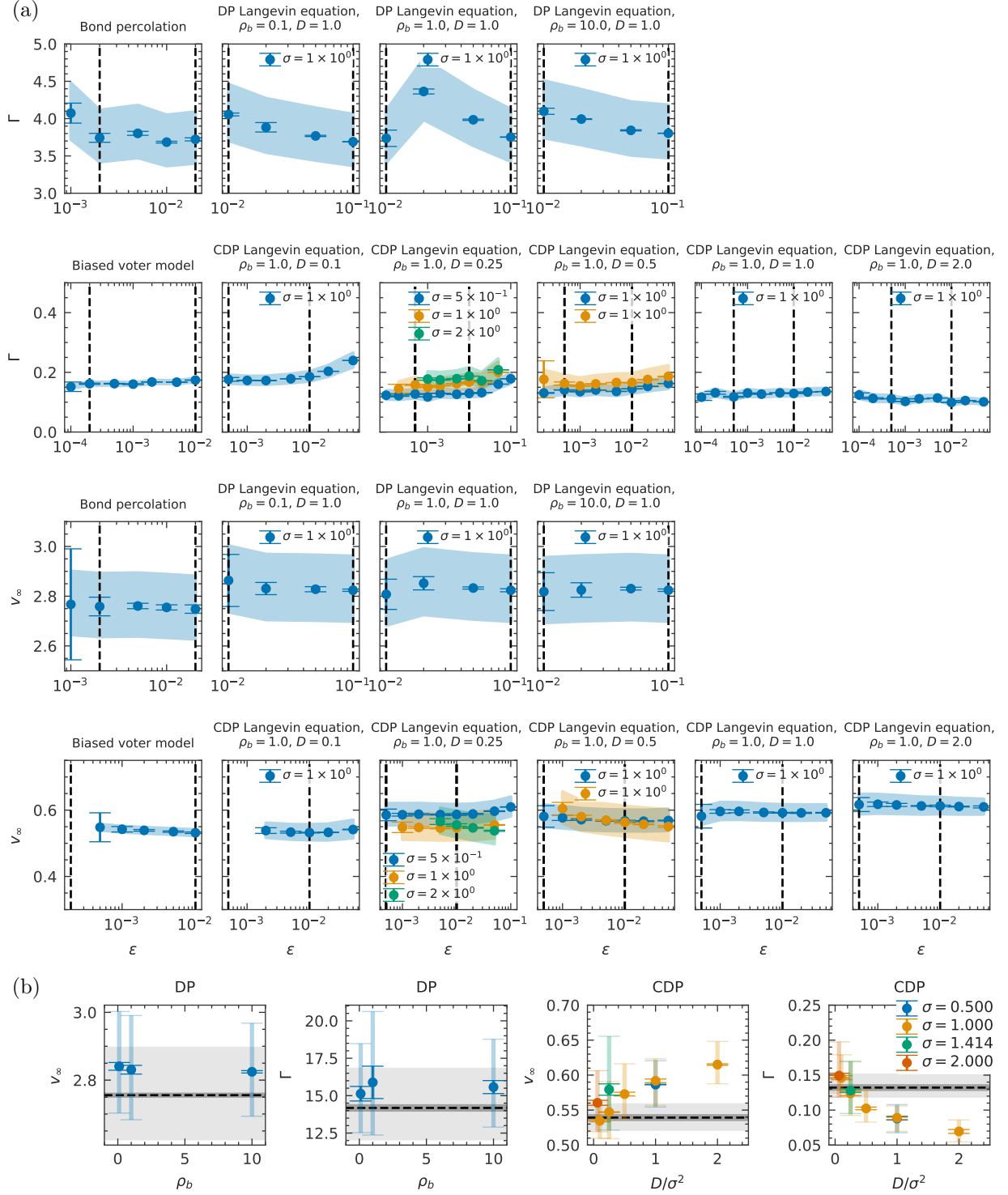
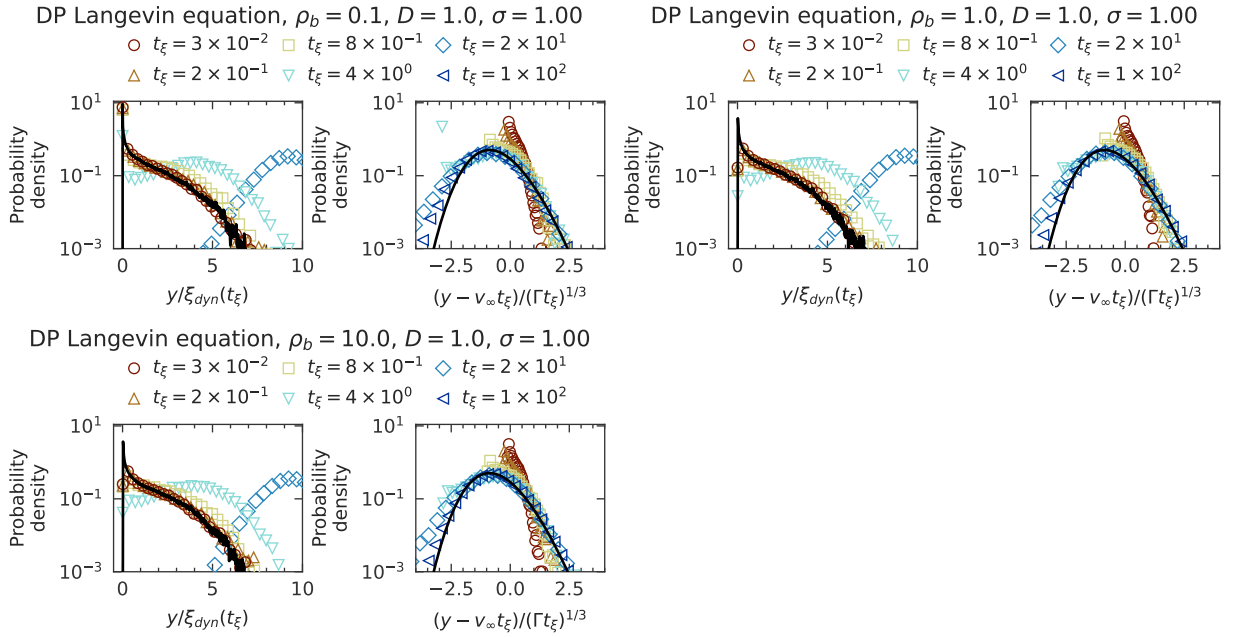
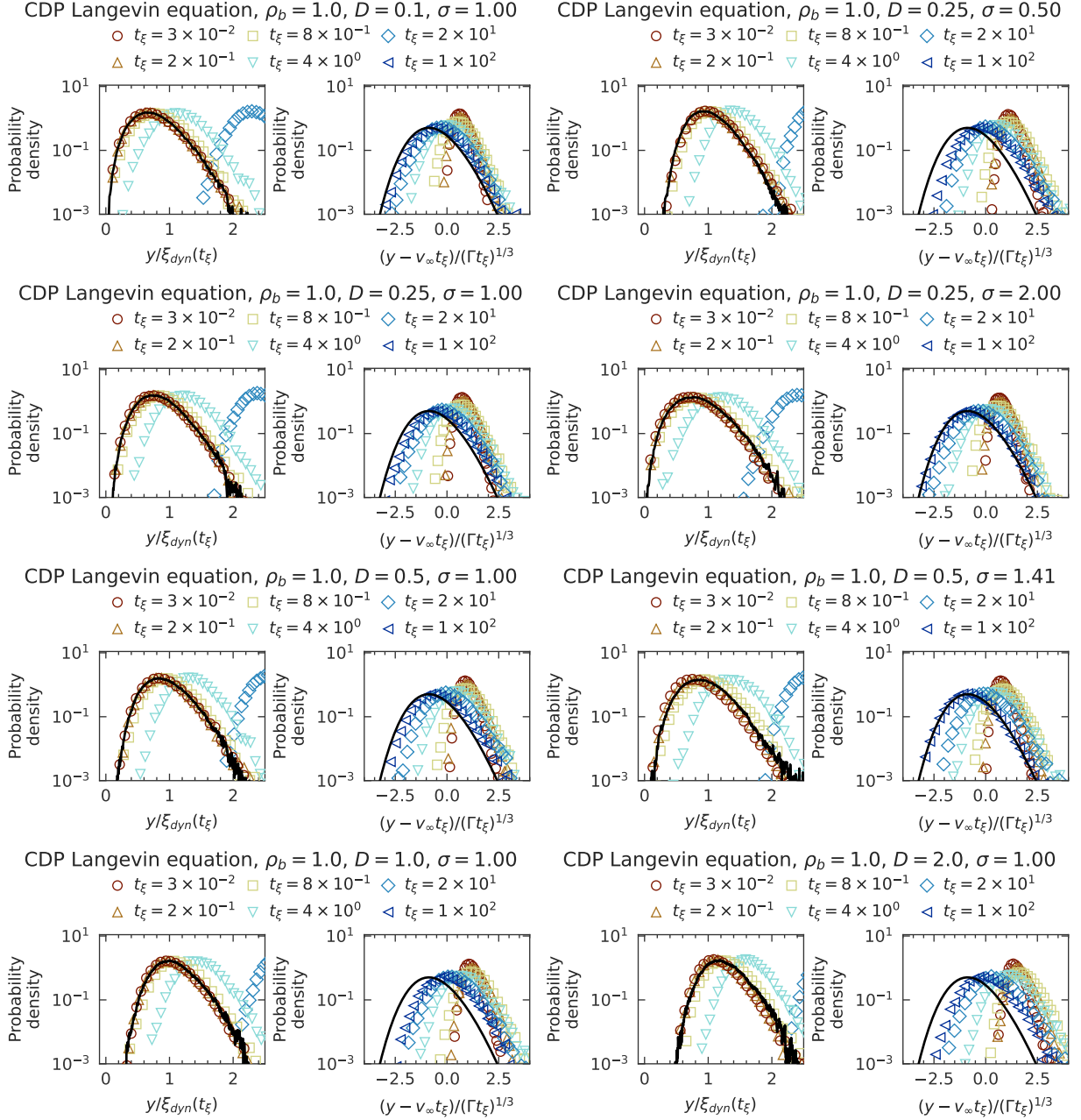


FIG. S18: Estimated parameters for the KPZ interfaces,  $v_\infty$  and  $\Gamma$ . Panel (a) shows the values for different  $\epsilon$ , and (b) shows the estimated values for  $\epsilon \rightarrow 0$ . The stochastic uncertainty and the systematic uncertainty due to the uncertainty in the nonuniversal parameter estimation are shown by the error bars and the shaded area in (a), and by the error bars with dark and light colors in (b), respectively. The  $\epsilon$  ranges used to estimate the values in (b) are indicated by two dashed lines in (a). In (b), the values, stochastic uncertainty, and systematic uncertainty for the DK models are shown by the dashed line, the dark gray shaded area, and the light gray shaded area, respectively. The parameters used in the simulations are summarized in Tables SIV and SV.





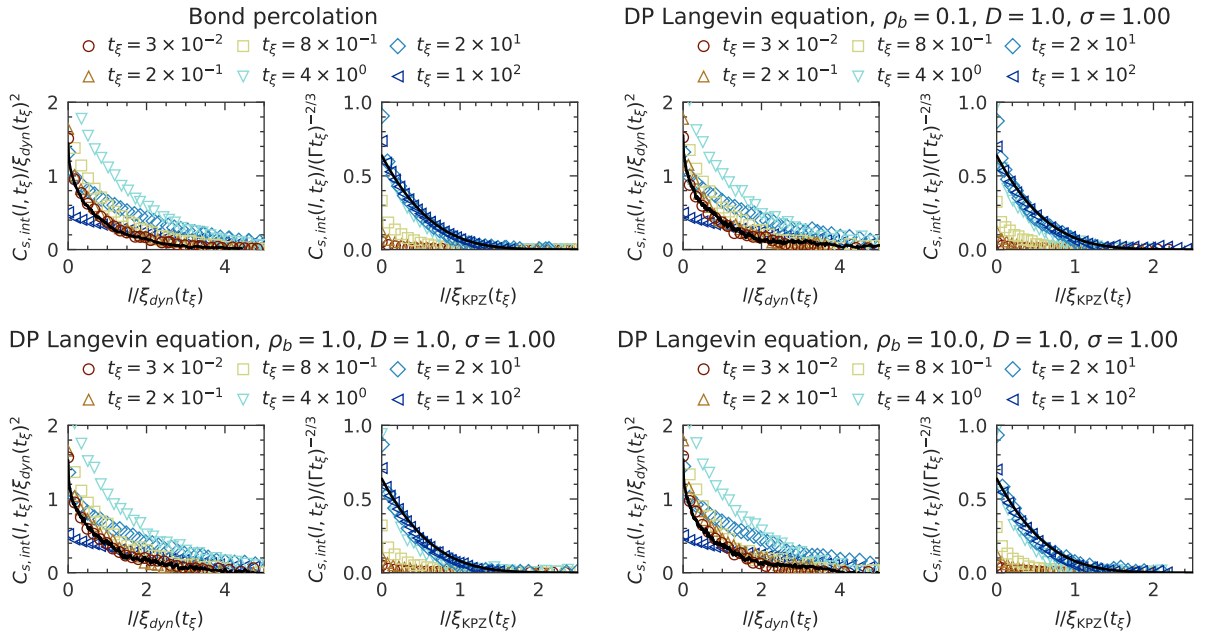


FIG. S21: Height spatial covariance for the DP models, plotted at different  $t_\xi$ . The black solid lines indicate the data for the critical case (left plots) and the exact solution for flat KPZ interfaces (right plots) [S5], respectively.

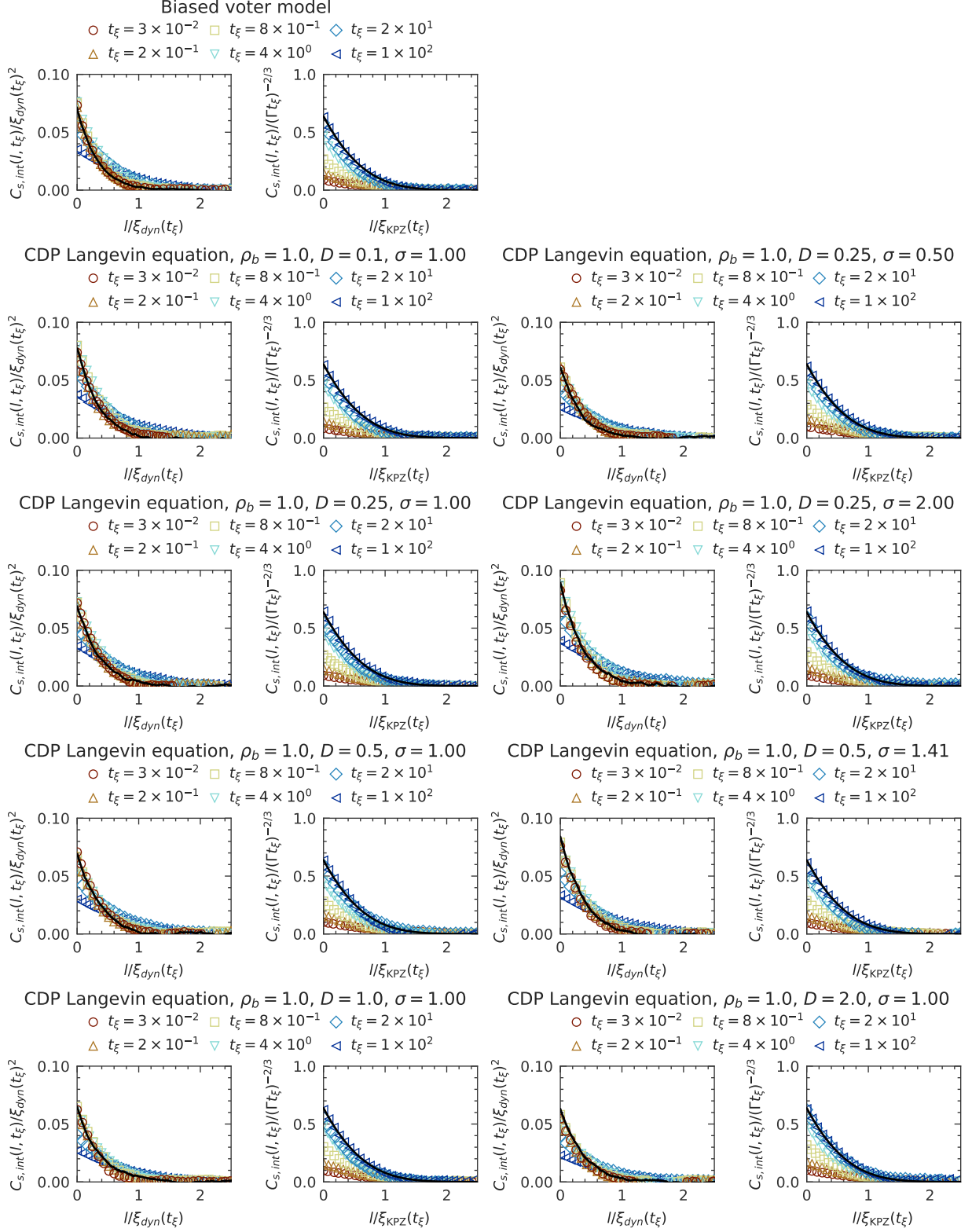


FIG. S22: Height spatial covariance for the CDP models, plotted at different  $t_\xi$ . The black solid lines indicate the data for the critical case (left plots) and the exact solution for flat KPZ interfaces (right plots) [S5], respectively.

---

\* ysk@yfukai.net

- S1 I. Dornic, H. Chaté, and M. A. Muñoz, Integration of Langevin Equations with Multiplicative Noise and the Viability of Field Theories for Absorbing Phase Transitions, *Physical Review Letters* **94**, 100601 (2005).
- S2 W. H. Press, S. A. Teukolsky, W. T. Vetterling, and B. P. Flannery, *Numerical Recipes 3rd Edition: The Art of Scientific Computing*, 3rd ed. (Cambridge University Press, Cambridge, UK ; New York, 2007).
- S3 M. Newville, R. Otten, A. Nelson, T. Stensitzki, A. In-gargiola, D. Allan, A. Fox, F. Carter, Michał, R. Osborn, D. Pustakhod, S. Weigand, lneuhaus, A. Aristov, Glenn, Mark, mgunyho, C. Deil, A. L. R. Hansen, G. Pasquevich, L. Foks, N. Zobrist, O. Frost, Stuermer, J.-C. Jaskula, S. Caldwell, P. Eendebak, M. Pompili, J. H. Nielsen, and A. Persaud, *Lmfit/lmfit-py*: 1.3.1, Zenodo (2024).
- S4 Theoretical curves available in the following URL were used: <https://www-m5.ma.tum.de/KPZ>.
- S5 F. Bornemann, On the numerical evaluation of fredholm determinants, *Math. Comput.* **79**, 871 (2010).